Antarctic Ice Sheet freshwater discharge drives substantial Southern Ocean changes over the 21st century

Tessa Gorte[1], Nicole Suzanne Lovenduski[1], Cara Nissen[1], and Jan Thérèse Maria Lenaerts[1]

[1]University of Colorado Boulder

June 25, 2023

Abstract

Multidecadal satellite observations indicate that the Antarctic Ice Sheet (AIS) is losing mass at an accelerating rate, potentially impacting many aspects of the coupled climate system. While previous studies have demonstrated the importance of AIS freshwater discharge for regional and global climate processes using climate model experiments, many have applied unrealistic freshwater forcing. Here, we explore the potential Southern Ocean impacts of realistic AIS mass loss over the 21st century in the Community Earth System Model version 2 (CESM2) by applying observation-based historical and ice sheet model-based future AIS freshwater forcing. The added freshwater reduces wintertime deep convective area by 72\% while retaining 83\% more sea ice. Congruent with other studies, we find the increased freshwater discharge extensively impacts local and remote Southern Ocean surface and subsurface temperature and stratification. These results demonstrate the necessity of accounting for AIS mass loss in global climate models for projecting future climate.

Antarctic Ice Sheet freshwater discharge drives substantial Southern Ocean changes over the 21st century

Tessa Gorte[1,2], Nicole Lovenduski[1,2], Cara Nisssen [1,2], Jan T. M. Lenaerts[1]

[1]Department of Atmospheric and Oceanic Sciences, University of Colorado Boulder, Boulder CO, USA
[2]Institute of Arctic and Alpine Research, University of Colorado Boulder, Boulder CO, USA

Key Points:

- We explore impacts of realistic Antarctic Ice Sheet (AIS) freshwater discharge on the Southern Ocean using a state-of-the-art climate model
- AIS discharge drives drastic changes in Southern Ocean stratification, winter deep convection, surface and interior temperature, and sea ice
- Our results suggest that regional AIS discharge can have far-reaching impacts on the Southern Ocean that can feedback on the climate system

Corresponding author: Tessa Gorte, `tessa.gorte@colorado.edu`

Abstract

Multidecadal satellite observations indicate that the Antarctic Ice Sheet (AIS) is losing mass at an accelerating rate, which has the potential to impact many aspects of the coupled climate system. While previous studies have demonstrated the importance of AIS freshwater discharge for regional and global climate processes using climate model experiments, many have applied unrealistic freshwater forcing. Here, we explore the potential Southern Ocean impacts of realistic AIS mass loss over the 21^{st} century in the Community Earth System Model version 2 (CESM2) by applying observation-based historical and ice sheet model-based future AIS freshwater forcing. The added freshwater reduces wintertime deep convective area by 72% while retaining 83% more sea ice. Congruent with other studies, we find the increased freshwater discharge extensively impacts local and remote Southern Ocean surface and subsurface temperature and stratification. These results demonstrate the necessity of accounting for AIS mass loss in global climate models for projecting future climate.

1 Introduction

Since the early 1990s, satellite-based observations have shown that the Antarctic Ice Sheet (AIS) is losing mass. The spatial pattern of AIS mass loss is heterogeneous (Rignot et al., 2019), mostly concentrated in the West Antarctic Ice Sheet (WAIS), which drains into the Amundsen and Bellingshausen Seas in the Southern Ocean (SO) (Velicogna & Wahr, 2006). The Ice sheet Mass Balance Inter-comparison Experiment version 2 (IMBIE2; Shepherd et al. (2018)) estimated that, from 1992-2017, the WAIS lost mass at a rate of 94 $\pm$ 27 Gt/y, and concluded that this mass loss has been accelerating (Rignot et al., 2019). Several studies using ice sheet models suggest that AIS mass loss will continue to accelerate in the future, as ice shelf thinning, grounding line retreat, and accelerating ice flow are all expected to continue and perhaps intensify with anthropogenic climate change(Pattyn & Morlighem, 2020; Gilbert & Kittel, 2021; Noble et al., 2020).

Apart from rising sea level (DeConto et al., 2021), AIS mass loss will affect many other aspects of the coupled climate system. Observations point to substantial physical changes in SO sea surface height, sea ice, water mass properties, and dense water formation, and a growing body of work attributes these changes to observed increases in AIS freshwater (FW) discharge (hereafter referred to as AIS discharge) (Jacobs & Giulivi, 2010; Fasullo & Nerem, 2018; Purich & England, 2023; Li et al., 2023). The SO's strong teleconnections to the global climate system mean that regional disruptions can precipitate broader changes elsewhere, across a range of timescales (Cabré & Gnanadesikan, 2017). Using climate model projections, previous work suggests that AIS FW fluxes will impact the future evolution of global atmospheric temperature and precipitation (Bronselaer et al., 2018), upper ocean stratification (Aiken & England, 2008; Swart & Fyfe, 2013), meridional overturning (Sadai et al., 2020; Moorman et al., 2020), and ocean temperature (Bintanja et al., 2015; Pauling et al., 2016; Park & Latif, 2019).

As AIS mass loss is not yet represented interactively in the latest generation of climate models, the potential impacts of AIS discharge on the coupled climate system are often investigated by directly applying anomalous FW fluxes to the ocean component of a climate model. Several studies apply FW forcing around AIS in a homogeneous fashion (Swart & Fyfe, 2013; Park & Latif, 2019; Purich & England, 2023) – inconsistent with the observed spatial pattern of AIS mass loss. Others aim to capture future melt of the large Ross and Ronne ice shelves, failing to reflect current grounded AIS mass loss (Bintanja et al., 2013, 2015). Pauling et al. (2016) explore potential impacts of spatially heterogeneous FW forcing but, like others (Aiken & England, 2008; Bintanja et al., 2013, 2015), impose FW abruptly with little to no gradual increase. Both Sadai et al. (2020) and Bronselaer et al. (2018) – which slowly increase the FW flux over several decades – employ global climate models (GCMs) from the Coupled Model Intercomparison Project version 5 (CMIP5) and apply a FW forcing based on CMIP5 Representative Concentration Pathway 8.5 (RCP8.5) runoff projections. These past studies have provided foundational understanding of the sensitivity of the climate system to large-scale AIS mass loss, but are unrealistic in representing the spatio-temporal variability in AIS mass changes and/or do not employ the latest versions of climate models (Landerer & Swenson, 2012).

Here, we apply a spatially heterogeneous FW signal that is reflective of the current spatial pattern of AIS mass loss that increases based on (1) satellite observations for the historical period and (2) CMIP6 Shared Socioeconomic Pathway 5-RCP8.5 (SSP5-8.5) runoff projections for the future period. Furthermore, we leverage the Community Earth System Model version 2 (CESM2), an Earth System Model from the updated suite of models in CMIP6. As we will demonstrate, the modeled Southern Ocean climate system is highly sensitive to AIS discharge – this discharge drives anomalous trends in vertical density stratification and surface and subsurface temperature as well as the seasonal cycles of sea ice and deep convective area. Furthermore, our results indicate that regional AIS discharge can impact these processes across the Southern Ocean basin.

2 Methods

In this paper, we run two fully coupled climate simulations using CESM2. CESM2 is a global climate model operated by the National Center for Atmospheric Research (NCAR), which we ran under historical CMIP6 greenhouse gas forcing from 1970-2015 and SSP5-8.5 greenhouse gas forcing from 2016-2100 with a $\sim 0.9 \times 1.25°$ horizontal resolution (Danabasoglu et al., 2020). The first simulation, CONTROL, runs from 1970-2100 with historical forcing through 2015 and SSP5-8.5 atmospheric forcing from 2016-2100. CESM2 preserves mass for the AIS via a mass threshold that, when exceeded, informs the model to transport excess mass to the nearest ocean grid cell as solid ice discharge. For our CONTROL simulation, we override this mechanism, and instead point the model to a prescribed runoff value of 2775 Gt y^{-1} (1 Gt = 1 Gigaton = 10^{12} kg) which is divided into six drainage basins with spatially variable FW discharge that is constant in time (Figure S1 illustrates the discharge from basal melt and calving assigned to each of the basins derived from Lenaerts et al. (2015)). The second simulation, IMBIE, branches off of the CONTROL simulation in 1992 and is run out to 2100 under the same forcing conditions. In the IMBIE simulation, AIS FW forcing initially has the same spatial pattern as the CONTROL but is allowed to change in time – we create a more realistic forcing that is observations-based for the historical period (1992-2020) and ice sheet modeling-based for the future period (2021-2100) (Rignot et al., 2019; DeConto & Pollard, 2016). For the observations-based forcing, we apply a linear fit to AIS mass balance data, amalgamated from various products by Rignot et al. (2019) such that FW discharge increases from 2775 in 1992 to $\sim$3160 Gt y^{-1} in 2020 (Figure S1). The future AIS FW forcing is based on output from DeConto et al. (2021) who use a combination of ice sheet and climate modeling to estimate the AIS contribution to global mean sea level out to 2300 under RCP8.5 atmospheric warming conditions. Their model output shows steady AIS mass balance through $\sim$2050 after which point, the AIS losses mass non-linearly. To reproduce their findings, our IMBIE FW forcing is constant in time from 2021-2050 and increases quasi-exponentially through 2100 ending at a value of 9280 Gt y^{-1} (Figure S1). Our AIS FW regime corresponds to a total AIS contribution to global mean sea level rise of just over 1 m by 2100. With observations currently indicating that the focus of AIS mass loss is in WAIS, we evenly distribute all of the additional AIS FW flux to the surface coastal grid cells in the co-located drainage basin in the Amundsen and Bellingshausen Seas (AB Seas; 95 °W to 145 °W) (Figure S1). We also subdivide our FW forcing into its solid (calving) and liquid (basal melt) components. Each basin has its own ratio of solid to liquid FW based on results from Depoorter et al. (2013) and these ratios are held constant for the entirety of the simulations (Figure S1). Over the AIS, calving and basal melt account for $\sim$48% and $\sim$52%, respectively.

For this paper, the SO is defined as the ocean south of 50 °S and we explore upper ocean stratification, deep convective area (DCA), surface and interior ocean temperature, and sea ice extent (SIE). We quantify upper ocean stratification as the difference of the potential density at 200 m and that at the surface ($\Delta\rho_{200-\mathrm{surf}} = \rho_{200} - \rho_{\mathrm{surf}}$) such that positive numbers correspond to higher densities at depth (i.e. stable stratification). DCA is calculated as the combined grid cell area under which the maximum mixed layer depth exceeds 50% of the bathymetry (Heuzé et al., 2013; Heuzé, 2021). As such, DCA is purely a metric for how well the water column is mixed. Its existence can be – but is not necessarily – related to the formation of precursors of Antarctic Bottom Water which ultimately depends on the density of the waters involved. CESM2 is one of the few CMIP6 models that accurately produces deep convection solely in the coastal regions (Heuzé, 2021). We define the surface ocean as the topmost vertical layer of the ocean model in CESM2 (10 m thick) and consider anything below the mixed layer (∼100-150 m) to be the interior ocean.

3 Results

4 Results

Meltwater changes the density structure of the SO, resulting in enhanced upper ocean stratification (Figure 1). The SO-averaged difference in stratification, $\Delta\rho_{200-\mathrm{surf}}$, increases for both simulations but significantly more so in the IMBIE simulation (1A). For the entire 1992-2100 simulation period, the IMBIE simulation $\Delta\rho_{200-\mathrm{surf}}$ increases by approximately 0.2 kg m^{-3} (44%) while the CONTROL simulation, by comparison, increases by 0.05 kg m^{-3} (16%). The difference in SO stratification between the two simulations is largely realized in the latter half of the 21st century with much of the increase in the IMBIE simulation occurring after 2070. The spatial realization of the enhanced stratification is such that the signal in the IMBIE is largely focused in the AB Seas region but also present in the Ross and Weddell Seas (Figure 1B-C). In these areas, the increase in stratification can be upwards of 1 kg m^{-3} which constitutes a first order of magnitude change on the historical mean state (Figure S1). Whereas, the CONTROL simulation shows no significant change in stratification over the course of the 21st century in these regions. Rather, the CONTROL simulation indicates a small increase in stratification in the open Southern Ocean, that is also captured in the IMBIE simulation (Figures 1B-C).

AIS discharge is associated with a significant reduction in Southern Ocean DCA (Figure 2). CESM2 develops deep convection in many Antarctic coastal regions in the historical simulation (Figure 2, yellow regions on map insets). Over the course of the century, both the CONTROL and IMBIE simulations project a decline in SO DCA from June through December, when DCA is at a maximum (Figure 2A). Austral winter DCA declines by 17% in the CONTROL simulation over the century, driven by anthropogenic changes other than AIS discharge (e.g., warming). Whereas, in the austral summer when the DCA is at a minimum, there is no statistically significant change in DCA over time or between simulations (Figure 2A). Including the effects of AIS discharge leads to a wintertime DCA reduction from a median value of 0.34 Mkm^2 to 0.24 Mkm^2; ∼29% (Figure 2A). Even with the 29% reduction in wintertime SO DCA in the IMBIE simulation, the median DCA for every month is within the extrema for the CONTROL(Figure 2A).

The AIS discharge-related reduction in SO DCA manifests most strongly in the AB Seas, where our model simulation projects a 75% decline in DCA in the austral winter months in the IMBIE simulation. Compared to a 13% decline in DCA for the CONTROL, this indicates substantially reduced seasonal DCA variability (Figure 2B). By the end of the century, the medians for the months of May as well as August through November are outside the extremes of the CONTROL DCA. The median CONTROL DCA in this region is also reduced from August-November but is within the historical DCA dis-

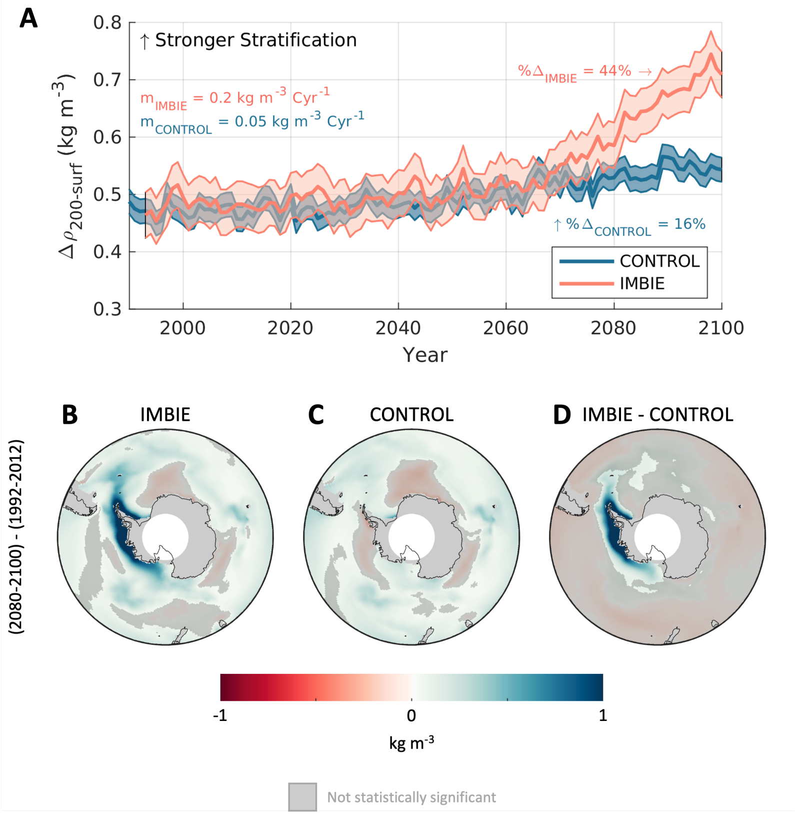

Figure 1. (A) Temporal evolution of the average SO potential density difference between the surface and 200 m depth ($\Delta\rho_{200-\mathrm{surf}}$) over 1990-2100 for both the CONTROL (blue) and IMBIE (peach) simulations. Larger numbers indicate stronger stratification. The solid line shows the SO average for each simulation and the shading indicates 1-σ. (B)-(C) End-of-century (2080-2100) minus beginning-of-century (1992-2012) $\Delta\rho_{200-\mathrm{surf}}$ in the IMBIE and CONTROL simulations, respectively. (D) Map of panel (B) - panel (C) showing the difference in the temporal evolution of stratification between the two simulations. Darker blues indicate stronger stratification with non-statistically significant changes shaded in grey.

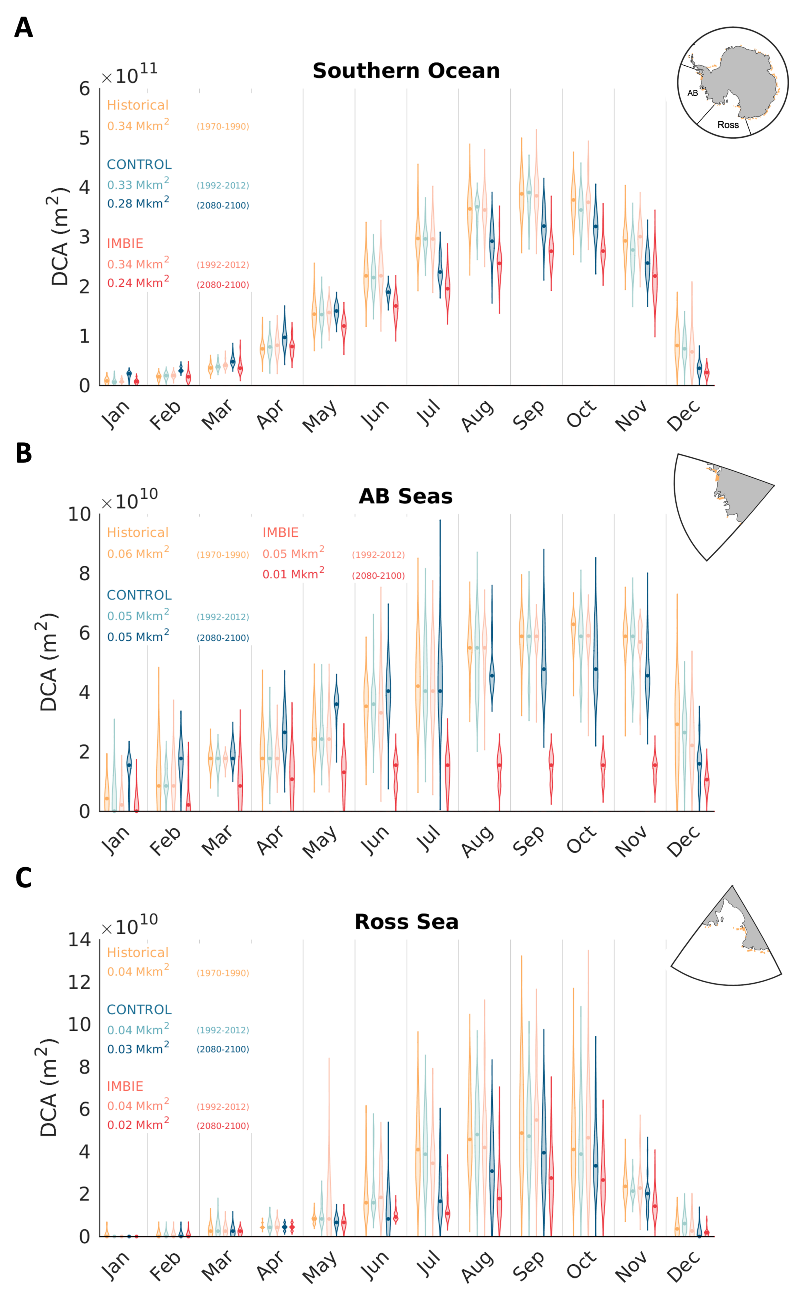

Figure 2. Monthly deep convective area climatology from the (yellow) 1970-1990 historical, (light blue) 1992-2012 CONTROL, (dark blue) 2080-2100 CONTROL, (peach) 1992-2012 IMBIE, and (red) 2080-2100 IMBIE periods/simulations averaged over the (A) Southern Ocean, (B) Amundsen/Bellingshausen Seas, and (C) Ross Sea regions. Maps in the upper right of each panel depict the region of interest as well as the historical DCA (yellow). The violin plots for each month represent the kernel density of DCA distribution. Each violin plot has a dot denoting the median DCA and the ends of the plot extend out to the extrema of the distribution.

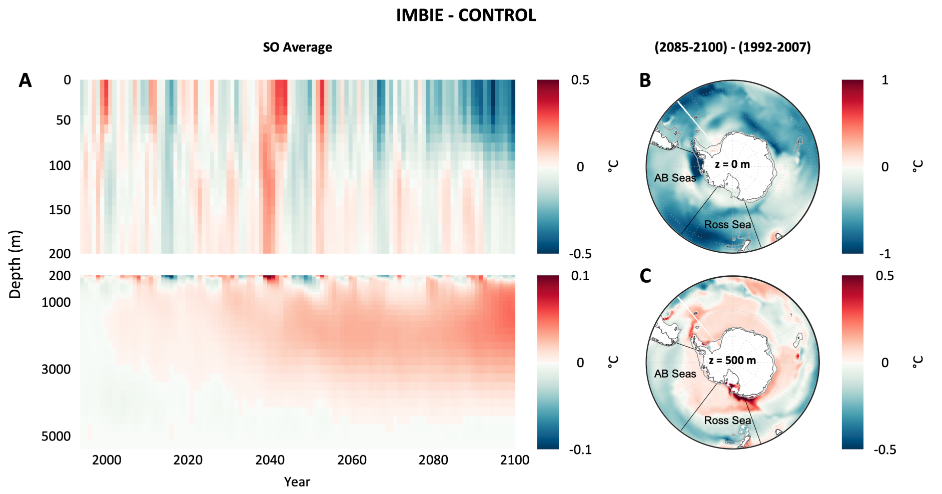

Figure 3. (A) The difference in average SO vertical temperature profile from 1992-2100 between the IMBIE and CONTROL simulations from 1992-2100. The upper panel depicts the top 200 m of the SO and has values ranging from -0.5 to 0.5 °C; the lower panel depicts 200 m to the ocean floor with values ranging from -0.1 to 0.1 °C. Bluer (redder) colors indicate when and at what depth the IMBIE simulation is cooler (warmer) than the CONTROL. (B) Difference (IMBIE-CONTROL) in SO surface temperature evolution comparing the 2080-2100 period to the 1992-2012 period. (C) Map of the difference (IMBIE-CONTROL) in SO 500 m depth temperature evolution comparing the 2080-2100 period to the 1992-2012 period. Black lines denote the boundaries of the AB Seas and Ross Sea regions.

tribution. The Ross Sea, whose DCA historically varies between ∼0.04-0.1 Mkm^2 in the austral winter and spring shows a 52% reduction in DCA in the IMBIE simulation and a 30% reduction in the CONTROL from July-November. The median IMBIE DCA is within the broad (and thus highly variable) historical distribution of DCA for the Ross Sea. As such, our simulations indicate that AIS discharge reduces deep convection both regionally in the AB Seas as well as in regions outside of where the FW forcing is applied, such as the Ross Sea.

AIS discharge leads to anomalous cooling in the surface and anomalous warming in the subsurface of the SO. The surface and subsurface SO warm ubiquitously in both simulations with anthropogenic climate change (Figure S3). The surface SO warms 0.28 °C less in the IMBIE simulation than in the CONTROL by 2100 (1.8 and 1.5 °C respectively). This anomalous cooling, which extends through the mixed layer (∼100 m), begins to appear mid-century, and intensifies after ∼2070 (Figure 3A). Anomalous surface ocean cooling in response to AIS discharge manifests most strongly in the AB Seas region, where we impose the strongest FW forcing (Figure 3B; Figure S1). Here, surface temperatures from the IMBIE simulation are nearly 2 °C cooler than those in the CONTROL simulation. Another area of anomalous cooling due to FW input manifests off the coast of the East AIS near Enderby Land; a region of low SIE.

In contrast to the surface cooling, the deep SO (500 - 3000 m) experiences anomalous warming with AIS discharge over the course of the century. Averaged over the SO, the IMBIE simulation warms by 0.70 °C compared to 0.63 °C in the CONTROL. As such, the IMBIE simulation is 0.07 °C warmer than the CONTROL on average between 500-3000 m depth by the end of the century (Figure 3A). The anomalous warming of the deep Southern Ocean is spatially heterogeneous. Figure 3C shows anomalously warm temperatures (~0.01 °C) extending from the coast northward to the core of the Antarctic Circumpolar Current, with much larger anomalies (0.89°C) in the Ross Sea and along the Adélie Coast at 500m. Notably, this pocket of anomalously warm water is not co-located with the AIS FW input.

Both simulations show an overall loss of sea ice over the 21st century with anthropogenic climate change, however, the IMBIE simulation shows significantly less extensive sea ice loss, especially in the austral winter/spring (July-November). The historical SO sea ice cover is largely circumpolar with the highest concentrations in the Weddell and Ross Seas (Figure 4A). By the end of the century (2080-2100) the IMBIE simulation retains over 50% more sea ice in the AB Seas region (Figure 4B). The Weddell and Ross Seas – particularly out at the sea ice edge near the peninsula – also preserve over 25% more sea ice than the CONTROL (Figure 4B). Historical SIE typically reaches an annual maximum in September-October and an annual minimum between February-March and can vary between 2-15 Mkm^2, seasonally, across the entire SO (Figure 4D). In the AB Seas, SIE varies between 0.25-3.25 Mkm^2. For both the AB Seas as well as the entire SO, there is a significant decline in SIE from the 1992-2012 period to the 2080-2100 period, driven by anthropogenic climate change (Figure 4C-D). However, there is a significant difference in SIE between the IMBIE and CONTROL simulations by the end of the century, particularly in the austral winter and spring (Figure 4C-D). For five months out of the year, the IMBIE simulation produces over 1 Mkm^2 more total SO sea ice than the CONTROL in the 2080-2100 period with the maximum, 1.3 Mkm^2 in September, equivalent to ~9% of the total historical SIE (Figure 4C). This disparity in SIE is largely due to more sea ice preservation in the AB Seas region, which retains nearly 20% more sea ice in the IMBIE simulation compared to the CONTROL (Figure 4D).

5 Conclusions and Discussion

To investigate the potential role of projected AIS discharge on the SO, we conducted analysis using two fully coupled climate simulations with identical atmospheric forcing but different AIS FW fluxes. AIS discharge anomalously increases upper ocean stratification by ~30% across the Southern Ocean, with large increases in the AB Seas, and smaller increases in the Weddell and Ross Seas. End-of century Southern Ocean wintertime deep convective area is 0.34 Mkm^2 in the control simulation, but only 0.24 Mkm^2 in the IMBIE simulation. Regionally, we see the strongest impacts in the AB Seas region as wintertime DCA is reduced to summertime levels while DCA in the Ross Sea declines by ~22% due to the FW. The IMBIE surface ocean is 0.28 °C cooler than that of the CONTROL while the subsurface warms significantly with warmer regions focused in the western Ross Sea and along the Adélie Land coast. Our simulations also project that the freshening and anomalous cooling of the surface SO induce conditions more favorable for sea ice formation.

Our results suggest that the freshening of the AB seas, and to a lesser extent, the broader Southern Ocean, is the primary driver of the enhanced stratification in the IMBIE simulation. Surface temperature cools while subsurface temperature warms in response to AIS discharge, a change that would induce reduced stratification if no salinity anomalies were present. The freshening and anomalous cooling of the surface SO induce conditions more favorable for sea ice formation. Previous studies have noted the importance of the ice-albedo feedback wherein when sea ice melts, it exposes the darker surface ocean below, lowering the albedo, increasing ocean heat uptake, inducing more sea ice melt and/or less sea ice growth (Curry et al., 1995). With the IMBIE simulation preserving more sea ice than the CONTROL, this positive feedback loop is suppressed, and the surface ocean is relatively cooler. When sea ice forms, however, it releases heat and rejects the oceanic brine, increasing the surface temperature and salinity, and thus inducing a negative feedback loop. The lower surface temperature and salinity in the IM-

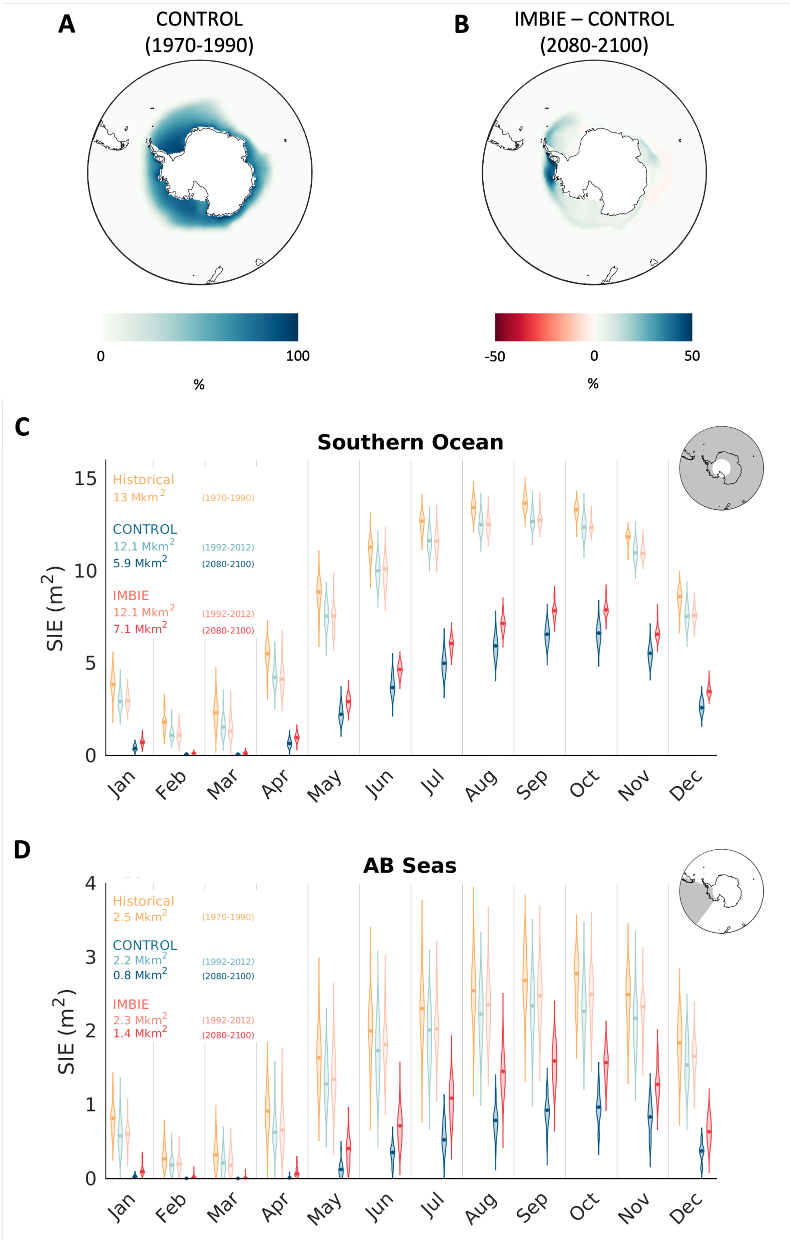

Figure 4. (A) Average annual mean of SIF in each grid cell for the 1970-1990 historical period. (B) the average difference in SIF between the IMBIE and CONTROL simulations during the 2080-2100 period. (C) Monthly SIE for the whole SO in the historical (yellow), 1992-2012 CONTROL (light blue), 2080-2100 CONTROL (dark blue), 1992-2012 IMBIE (peach), and 2080-2100 IMBIE (red) periods. The violin plots for each month represent the kernel density of SIE distribution. Each violin plot has a dot denoting the median SIE and the ends of the plot extend out to the extrema of the distribution.

BIE simulation, then, implies that the heat uptake (or lack thereof) and the FW discharge dominate the sea ice formation signal for the evolution of both variables. FW-induced changes to stratification and DCA as well as surface and interior temperature all permeate into more remote regions of the SO, mainly the Ross and Weddell Seas. Deep convection, which only occurs in coastal grid cells, is most strongly affected in the AB Seas but also manifests remotely in the Ross Sea. The loss in DCA is realized predominantly from July-November such that the historical wintertime high is reduced to summertime low levels in the AB Seas. This period aligns with that of the highest sea ice retention – most of the preserved sea ice exists in the AB Seas and, to a lesser extent, the Ross and Weddell Seas.

Our findings are supported by those reported in other studies. Compared to Bronselaer et al. (2018), Sadai et al. (2020), and Purich and England (2023), our SIE and surface and interior temperature manifest similarly in strength and spatial pattern with much of the AB Seas sea ice persisting despite strong anthropogenic warming and anomalous warming of the western Ross Sea. We find the sea ice response to be significantly less than what was found in the ice-shelf specific sensitivity experiments of Bintanja et al. (2013) and Bintanja et al. (2015). While we do see a differential sea ice response by the end of the century, the FW-induced changes are not statistically significantly different until after 2070; nearly 80 years into the simulation. As such, we find the minimal sea ice response in extent and trend over <50 model years as seen by Swart and Fyfe (2013) and Pauling et al. (2016), respectively, to be consistent with our results. Bintanja et al. (2013) find that the strength of their FW forcing engenders a sea ice response strong enough to account for the disparate observed SO sea ice cover. Our historical SO sea ice cover, which peaks at ∼15 Mkm^2 in September, is already lower than the observed 18-20 Mkm^2 in September SIE. Likely owing to anthropogenic warming, there is a significant overall reduction in SO SIE on the order of ∼5-8 Mkm^2 with the IMBIE simulation retaining ∼1 Mkm^2 more than the CONTROL by the end of the century. That is to say, the FW discharge does help preserve SO SIE but not enough to offset anthropogenic warming. Like Park and Latif (2019) and Li et al. (2023), we also see a decline in deep convection in the SO; both of which use models noted for producing too much open ocean deep convection (Heuzé, 2021).

There are three major caveats with this work: (1) the assumption that past observations are a good predictor of future changes, (2) the assumption of ice shelf mass (im)balance, and (3) the application of our FW forcing. We assume that past AIS melt patterns will continue into the future. Our understanding of the decades-to-centuries long spatio-temporal changes to AIS mass balance is limited, as mass change records from the GRACE satellite missions are only 20 years long. Ice sheet models – which are informed by these and other observations – project sustained elevated mass loss in the West AIS region over the course of the next century (DeConto & Pollard, 2016). Further, the GRACE satellites only measure the mass balance of the grounded ice sheet, not the ice shelves, leaving us with little information about large-scale ice shelf mass (im)balances across the AIS. In addition, CESM2 cannot model floating ice shelves. As such, we assume that the AIS ice shelves are in mass balance and that continental mass changes are directly realized as FW fluxes. These FW fluxes, then, are introduced solely to the coastal surface grid cells, though previous work indicates that similar GCMs are sensitive to neither the horizontal FW distribution close to or far from the coast nor the vertical FW distribution meaning our FW flux spatial distribution is reasonable for this assessment Bronselaer et al. (2018); Pauling et al. (2016). Finally, we leverage observed AIS mass changes from the GRACE satellites to guide historical (1992-2020) FW discharge and GCM output for future (2021-2100) discharge. The GCM (CESM1) projection we use for future AIS mass balance is (1) based on a model that doesn't have an active ice sheet and, thus, inherently misses any feedbacks with the coupled climate system and (2) generally constant until about 2050, after which point, it increases dramatically (DeConto et al., 2021).

Stitching these two forcings together, then, means that from 2021-2050, there is a constant annual FW forcing from the AIS that is guided by limited information.

Our results nevertheless demonstrate the potential ramifications of AIS FW discharge on the climate system. AIS FW is likely to play a key role in the spatio-temporal evolution of the SO over the 21st century. Given the importance of the SO for the uptake of anthropogenic heat and carbon (Frölicher et al., 2015), it is reasonable to expect that AIS FW discharge will engender climate feedbacks in the coming century and beyond.

6 Open Research

Data from the CONTROL simulation presented in this paper are publicly available at https://doi.org/10.5281/zenodo.8056558 (Gorte et al., 2023a). Data from the IMBIE simulation presented in this paper are publicly available at https://doi.org/10.5281/zenodo.8058223 (Gorte et al., 2023b).

Acknowledgments

We would like to thank Dr. Leo van Kampenhout for his work in the setup of these experiments.

This work was performed at the University of Colorado Boulder and Institute of Arctic and Alpine Research and was supported by the NASA's Sea Level Change Team (award #80NSSC20K1123). We would also like to acknowledge NCAR's Land Ice and Polar Climate Working Groups for their valuable computing time contributions.

References

Aiken, C. M., & England, M. H. (2008, 8). Sensitivity of the present-day climate to freshwater forcing associated with antarctic sea ice loss. *Journal of Climate*, *21*, 3936-3946. doi: 10.1175/2007JCLI1901.1

Bintanja, R., Oldenborgh, G. J. V., Drijfhout, S. S., Wouters, B., & Katsman, C. A. (2013, 5). Important role for ocean warming and increased ice-shelf melt in antarctic sea-ice expansion. *Nature Geoscience*, *6*, 376-379. doi: 10.1038/NGEO1767

Bintanja, R., Oldenborgh, G. J. V., & Katsman, C. A. (2015). The effect of increased fresh water from antarctic ice shelves on future trends in antarctic sea ice. *Annals of Glaciology*, *56*, 120-126. doi: 10.3189/2015AOG69A001

Bronselaer, B., Winton, M., Griffies, S. M., Hurlin, W. J., Rodgers, K. B., Sergienko, O. V., ... Russell, J. L. (2018, 11). Change in future climate due to antarctic meltwater. *Nature 2018 564:7734*, *564*, 53-58. Retrieved from `https://www.nature.com/articles/s41586-018-0712-z` doi: 10.1038/s41586-018-0712-z

Cabré, A., & Gnanadesikan, A. (2017). Global atmospheric teleconnections and multidecadal climate oscillations driven by southern ocean convection. Retrieved from `www.ametsoc.org/PUBSReuseLicenses` doi: 10.1175/JCLI-D-16-0741.s1

Curry, J. A., Schramm, J. L., & Ebert, E. E. (1995). Sea ice-albedo climate feedback mechanism. *Journal of Climate*, *8*, 240 - 247. Retrieved from `https://journals.ametsoc.org/view/journals/clim/8/2/1520-0442_1995_008_0240_siacfm_2_0_co_2.xml` doi: https://doi.org/10.1175/1520-0442(1995)008⟨0240:SIACFM⟩2.0.CO;2

Danabasoglu, G., Lamarque, J. F., Bacmeister, J., Bailey, D. A., DuVivier, A. K., Edwards, J., ... Strand, W. G. (2020, 2). The community earth system model version 2 (cesm2). *Journal of Advances in Modeling Earth Systems*, *12*, e2019MS001916. Retrieved from https://onlinelibrary.wiley.com/doi/full/10.1029/2019MS001916https://onlinelibrary.wiley.com/doi/abs/10.1029/2019MS001916https://agupubs.onlinelibrary.wiley.com/doi/10.1029/2019MS001916 doi: 10.1029/2019MS001916

DeConto, R. M., & Pollard, D. (2016, 3). Contribution of antarctica to past and future sea-level rise. *Nature*, *531*, 591-597. doi: 10.1038/nature17145

DeConto, R. M., Pollard, D., Alley, R. B., Velicogna, I., Gasson, E., Gomez, N., . . . Dutton, A. (2021, 5). The paris climate agreement and future sea-level rise from antarctica. *Nature 2021 593:7857*, *593*, 83-89. Retrieved from https://www.nature.com/articles/s41586-021-03427-0 doi: 10.1038/s41586-021-03427-0

Depoorter, M. A., Bamber, J. L., Griggs, J. A., Lenaerts, J. T., Ligtenberg, S. R., Broeke, M. R. V. D., & Moholdt, G. (2013). Calving fluxes and basal melt rates of antarctic ice shelves. *Nature*, *502*, 89-92. doi: 10.1038/nature12567

Fasullo, J. T., & Nerem, R. S. (2018, 12). Altimeter-era emergence of the patterns of forced sea-level rise in climate models and implications for the future. *Proceedings of the National Academy of Sciences of the United States of America*, *115*, 12944-12949. doi: 10.1073/pnas.1813233115

Frölicher, T. L., Sarmiento, J. L., Paynter, D. J., Dunne, J. P., Krasting, J. P., & Winton, M. (2015). Dominance of the southern ocean in anthropogenic carbon and heat uptake in cmip5 models. *Journal of Climate*, *28*, 862-886. doi: 10.1175/JCLI-D-14-00117.1

Gilbert, E., & Kittel, C. (2021, 4). Surface melt and runoff on antarctic ice shelves at 1.5°c, 2°c, and 4°c of future warming. *Geophysical Research Letters*, *48*, e2020GL091733. Retrieved from https://onlinelibrary.wiley.com/doi/full/10.1029/2020GL091733https://onlinelibrary.wiley.com/doi/abs/10.1029/2020GL091733https://agupubs.onlinelibrary.wiley.com/doi/10.1029/2020GL091733 doi: 10.1029/2020GL091733

Gorte, T., Lovenduski, N., Nissen, C., & Lenaerts, J. T. (2023a, June). *CESM2 CONTROL simulation output: Antarctic Ice Sheet freshwater discharge drives substantial Southern Ocean changes over the 21st century.* Zenodo. Retrieved from https://doi.org/10.5281/zenodo.8056558 doi: 10.5281/zenodo.8056558

Gorte, T., Lovenduski, N., Nissen, C., & Lenaerts, J. T. (2023b, June). *CESM2 IMBIE simulation output: Antarctic Ice Sheet freshwater discharge drives substantial Southern Ocean changes over the 21st century.* Zenodo. Retrieved from https://doi.org/10.5281/zenodo.8058223 doi: 10.5281/zenodo.8058223

Heuzé, C. (2021, 1). Antarctic bottom water and north atlantic deep water in cmip6 models. *Ocean Science*, *17*, 59-90. doi: 10.5194/os-17-59-2021

Heuzé, C., Heywood, K. J., Stevens, D. P., & Ridley, J. K. (2013, 4). Southern ocean bottom water characteristics in cmip5 models. *Geophysical Research Letters*, *40*, 1409-1414. doi: 10.1002/grl.50287

Jacobs, S. S., & Giulivi, C. F. (2010, 9). Large multidecadal salinity trends near the pacific-antarctic continental margin. *Journal of Climate*, *23*, 4508-4524. doi: 10.1175/2010JCLI3284.1

Landerer, F. W., & Swenson, S. C. (2012). Accuracy of scaled grace terrestrial water storage estimates. *Water Resources Research*, *48*. doi: 10.1029/2011WR011453

Lenaerts, J. T. M., Bars, D. L., van Kampenhout, L., Vizcaino, M., Enderlin, E. M., & van den Broeke, M. R. (2015, 8). Representing greenland ice sheet freshwater fluxes in climate models. *Geophysical Research Letters*, *42*, 6373-6381. Retrieved from http://doi.wiley.com/10.1002/2015GL064738 doi: 10.1002/2015GL064738

Li, Q., England, M. H., Hogg, A. M., Rintoul, S. R., & Morrison, A. K. (2023, 3). Abyssal ocean overturning slowdown and warming driven by antarctic meltwater. *Nature*, *615*, 841-847. Retrieved from https://www.nature.com/articles/s41586-023-05762-w doi: 10.1038/s41586-023-05762-w

Moorman, R., Morrison, A. K., & Hogg, A. M. C. (2020, 8). Thermal responses to antarctic ice shelf melt in an eddy-rich global ocean-sea ice model. *Journal of Climate*, *33*, 6599-6620. doi: 10.1175/JCLI-D-19-0846.1

Noble, T. L., Rohling, E. J., Aitken, A. R., Bostock, H. C., Chase, Z., Gomez, N., ... Williams, T. (2020, 12). The sensitivity of the antarctic ice sheet to a changing climate: Past, present, and future. *Reviews of Geophysics*, *58*, e2019RG000663. Retrieved from https://onlinelibrary.wiley.com/doi/full/10.1029/2019RG000663https://onlinelibrary.wiley.com/doi/abs/10.1029/2019RG000663https://agupubs.onlinelibrary.wiley.com/doi/10.1029/2019RG000663 doi: 10.1029/2019RG000663

Park, W., & Latif, M. (2019, 3). Ensemble global warming simulations with idealized antarctic meltwater input. *Climate Dynamics*, *52*, 3223-3239. doi: 10.1007/s00382-018-4319-8

Pattyn, F., & Morlighem, M. (2020, 3). The uncertain future of the antarctic ice sheet. *Science*, *367*, 1331-1335. Retrieved from https://www.science.org/doi/10.1126/science.aaz5487 doi: 10.1126/SCIENCE.AAZ5487/ASSET/D0DE1D3F-7990-45CB-9D79-D9B922FD6075/ASSETS/GRAPHIC/367_1331_F4.JPEG

Pauling, A. G., Bitz, C. M., Smith, I. J., & Langhorne, P. J. (2016). The response of the southern ocean and antarctic sea ice to freshwater from ice shelves in an earth system model. *Journal of Climate*, *29*, 1655-1672. doi: 10.1175/JCLI-D-15-0501.1

Purich, A., & England, M. H. (2023, 1). Projected impacts of antarctic meltwater anomalies over the twenty-first century. *Journal of Climate*, *36*, 2703-2719. doi: 10.1175/jcli-d-22-0457.1

Rignot, E., Mouginot, J., Scheuchl, B., van den Broeke, M., van Wessem, M. J., & Morlighem, M. (2019). Four decades of antarctic ice sheet mass balance from 1979–2017. *Proceedings of the National Academy of Sciences*, *116*, 1095-1103. doi: 10.1073/pnas.1812883116

Sadai, S., Condron, A., DeConto, R., & Pollard, D. (2020, 9). Future climate response to antarctic ice sheet melt caused by anthropogenic warming. *Science Advances*, *6*, eaaz1169. Retrieved from http://advances.sciencemag.org/ doi: 10.1126/sciadv.aaz1169

Shepherd, A., Ivins, E., Rignot, E., Smith, B., Broeke, M. V. D., Velicogna, I., ... Wouters, B. (2018, 6). *Mass balance of the antarctic ice sheet from 1992 to 2017* (Vol. 558). Nature Publishing Group. doi: 10.1038/s41586-018-0179-y

Swart, N. C., & Fyfe, J. C. (2013, 8). The influence of recent antarctic ice sheet retreat on simulated sea ice area trends. *Geophysical Research Letters*, *40*, 4328-4332. doi: 10.1002/GRL.50820

Velicogna, I., & Wahr, J. (2006, 3). Measurements of time-variable gravity show mass loss in antarctica. *Science*, *311*, 1754-1756. Retrieved from https://www.science.org/doi/10.1126/science.1123785 doi: 10.1126/SCIENCE.1123785/ASSET/930F3A74-2360-4753-ADB9-8ED78286A1F8/ASSETS/GRAPHIC/311_1754_F3.JPEG

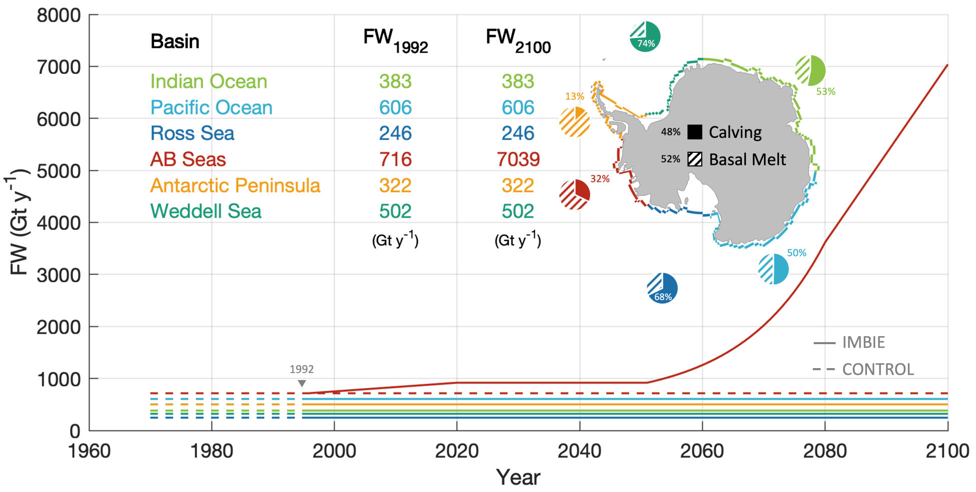

Figure S1. The AIS FW distribution shown spatially and as a time series. The 6 basins we define are the Weddell Sea (dark green), the Indian Ocean (light green), the Pacific Ocean (light blue), the Ross Sea (dark blue), the AB Seas (red), and the Antarctic Peninsula (orange). Each basin has its own ratio of calving to basal melt as depicted by the pie charts (percentages denote the percent of FW flux realized as calving). The time series show the total FW fluxing from each basin for the CONTROL (dashed) and the IMBIE (solid) simulations; the latter of which branches off in 1992. Also displayed are the values of total FW fluxing from each basin in 1992 and in 2100 in Gt y^{-1}.

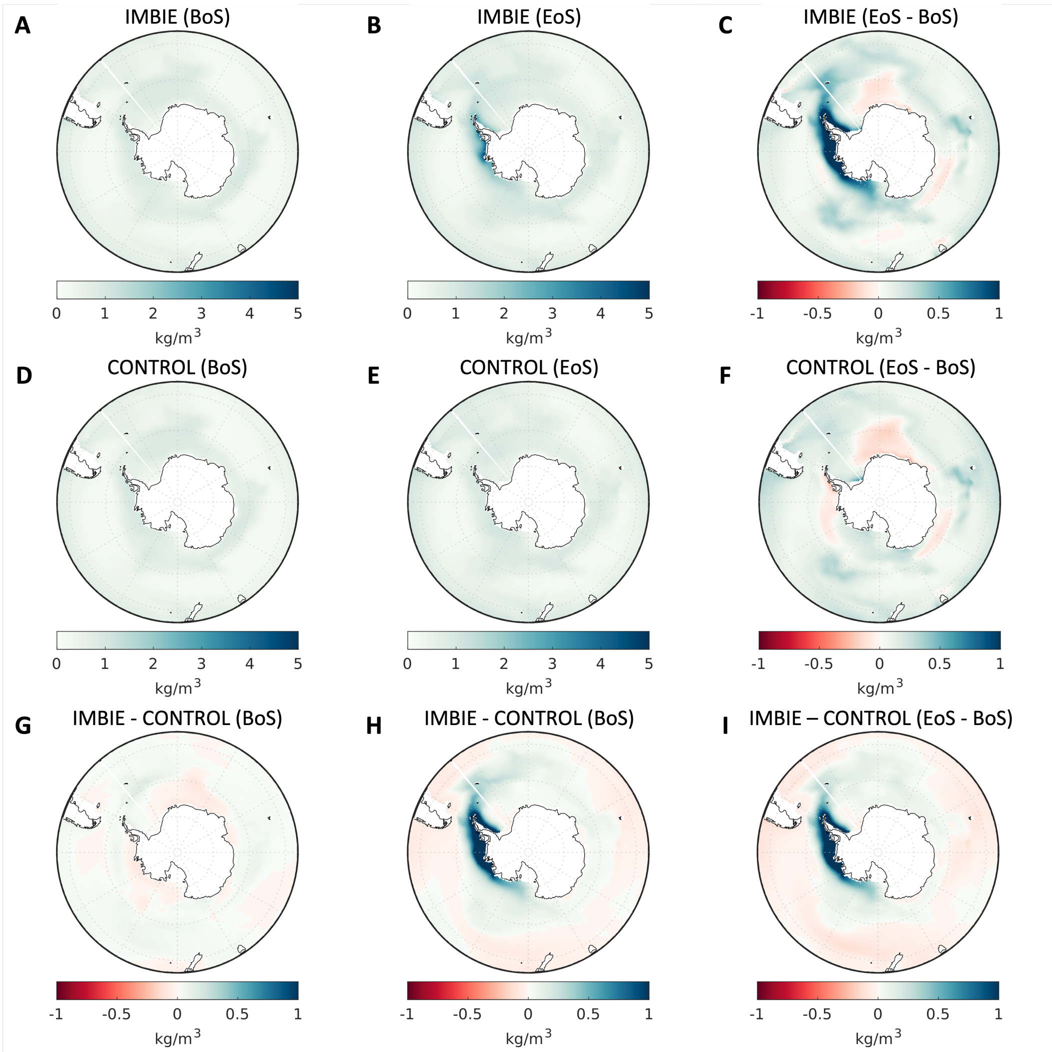

Figure S2. Snapshots of density stratification (200 m - surface) for the IMBIE simulation (top row), CONTROL simulation (middle row), and the difference (IMBIE - CONTROL; bottom row). The columns depict the average stratification for the periods of 1992-2007 (left), 2085-2100 (center), and the difference (right).

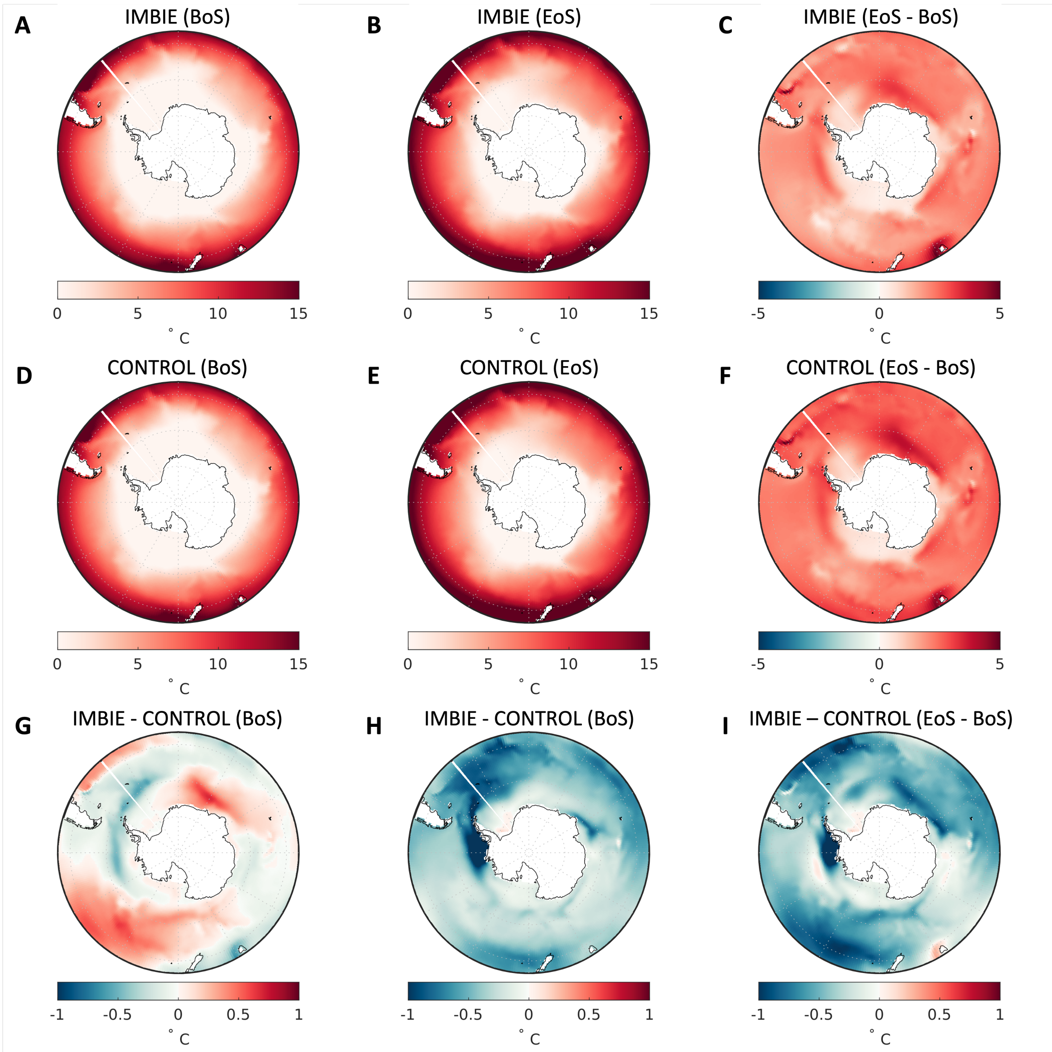

Figure S3. Snapshots of surface temperature for the IMBIE simulation (top row), CONTROL simulation (middle row), and the difference (IMBIE - CONTROL; bottom row). The columns depict the average surface temperature for the beginning of the simulation (BoS) from 1992-2007 (left), the end of the simulation (EoS) 2085-2100 (center), and the difference (right).

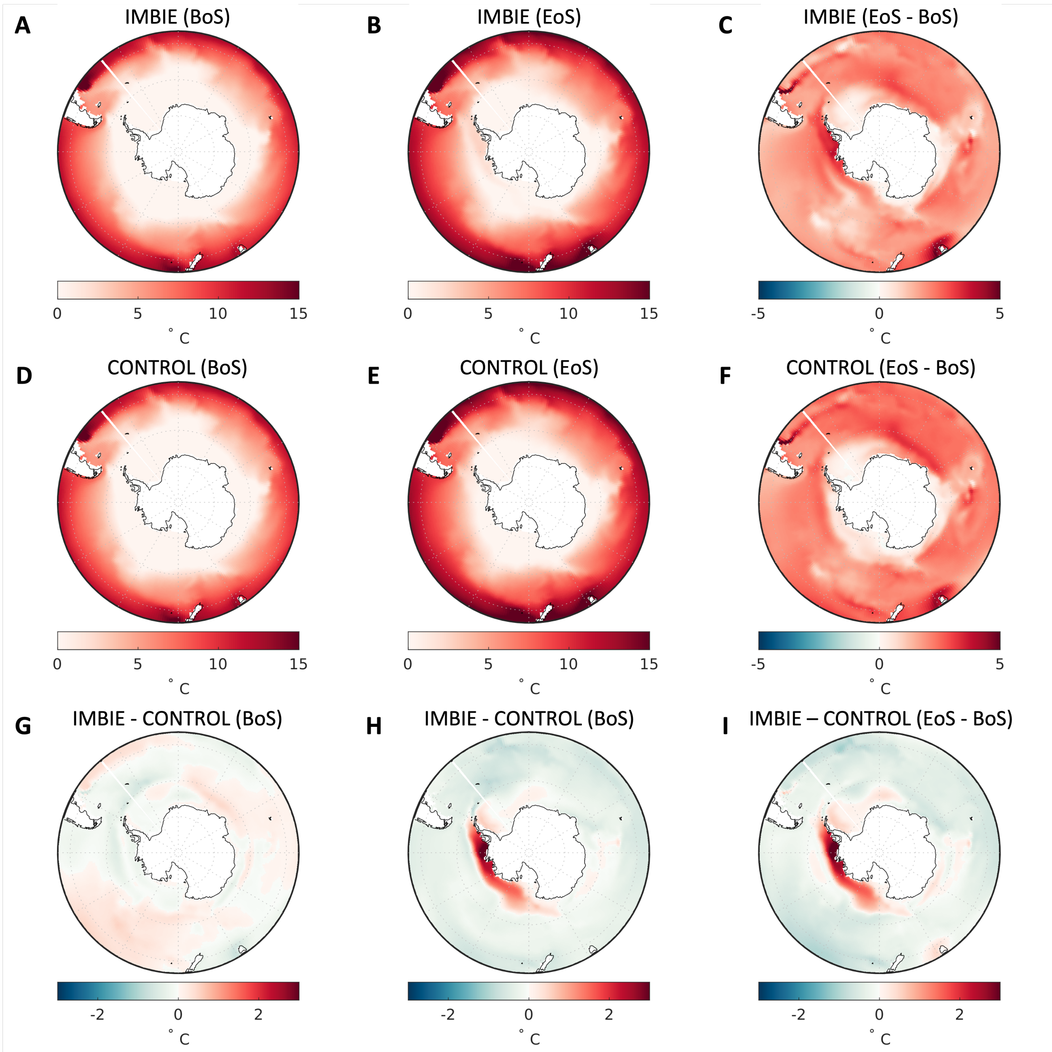

Figure S4. Snapshots of T_{100} for the IMBIE simulation (top row), CONTROL simulation (middle row), and the difference (IMBIE - CONTROL; bottom row). The columns depict the average T_{100} for the beginning of the simulation (BoS) from 1992-2007 (left), the end of the simulation (EoS) 2085-2100 (center), and the difference (right).

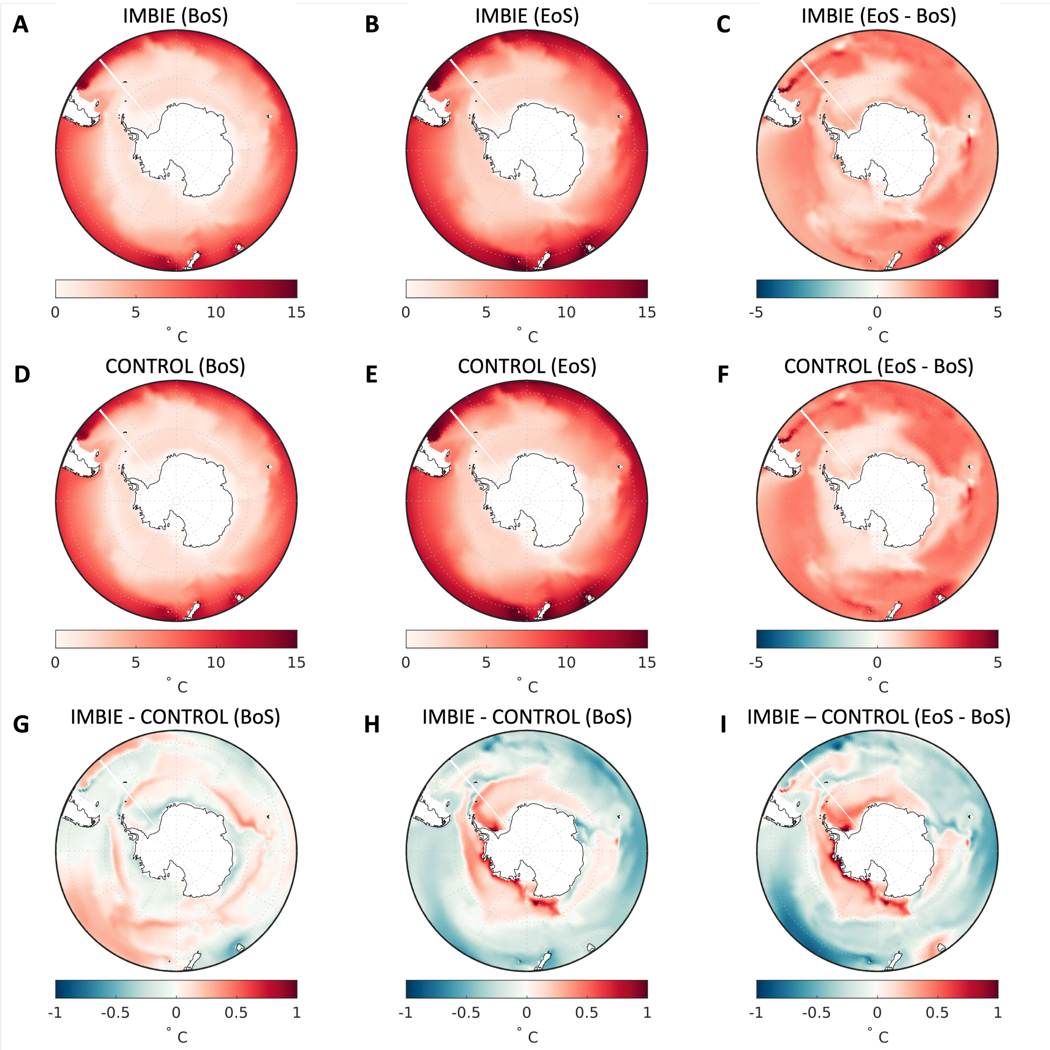

Figure S5. Snapshots of T_{200} for the IMBIE simulation (top row), CONTROL simulation (middle row), and the difference (IMBIE - CONTROL; bottom row). The columns depict the average T_{200} for the beginning of the simulation (BoS) from 1992-2007 (left), the end of the simulation (EoS) 2085-2100 (center), and the difference (right).

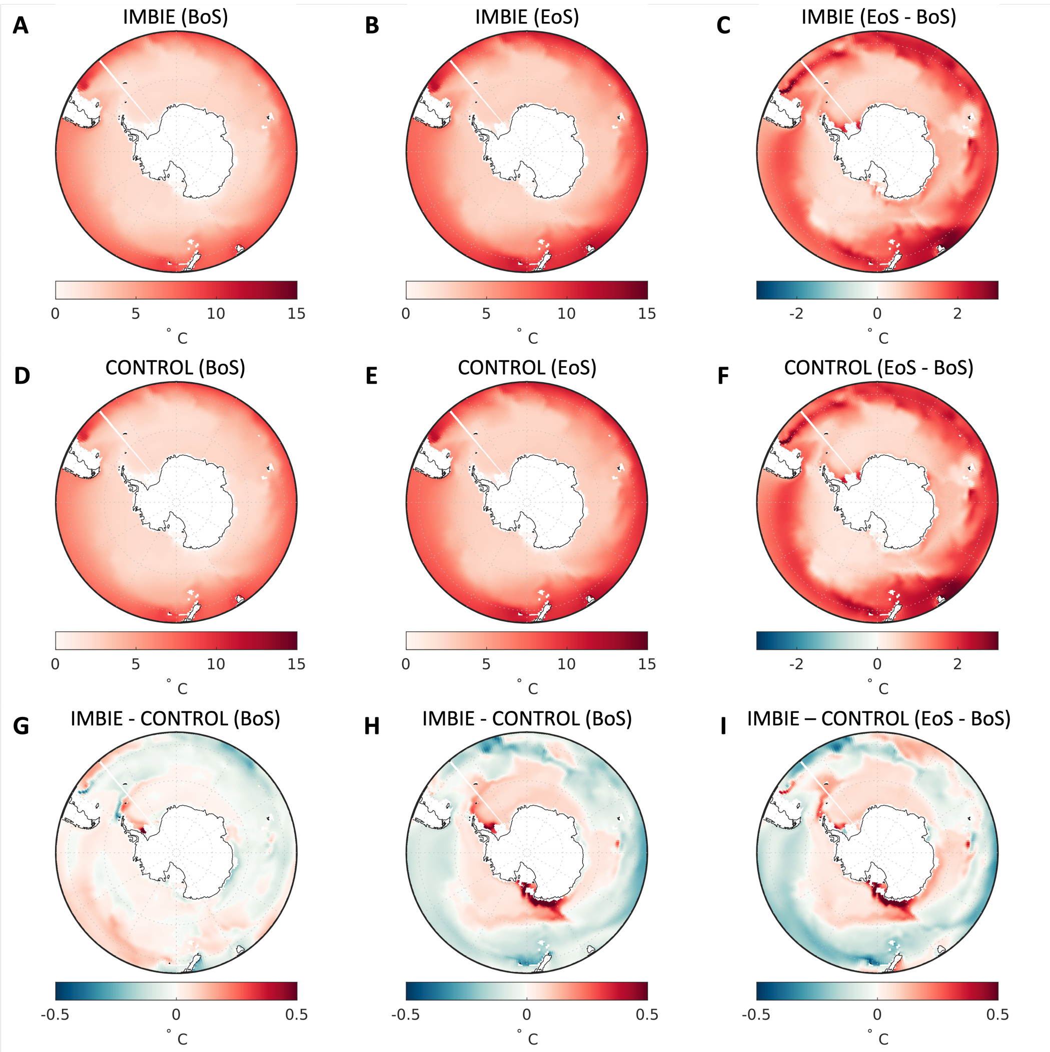

Figure S6. Snapshots of T_{500} for the IMBIE simulation (top row), CONTROL simulation (middle row), and the difference (IMBIE - CONTROL; bottom row). The columns depict the average T_{500} for the beginning of the simulation (BoS) from 1992-2007 (left), the end of the simulation (EoS) 2085-2100 (center), and the difference (right).

Figure 1.

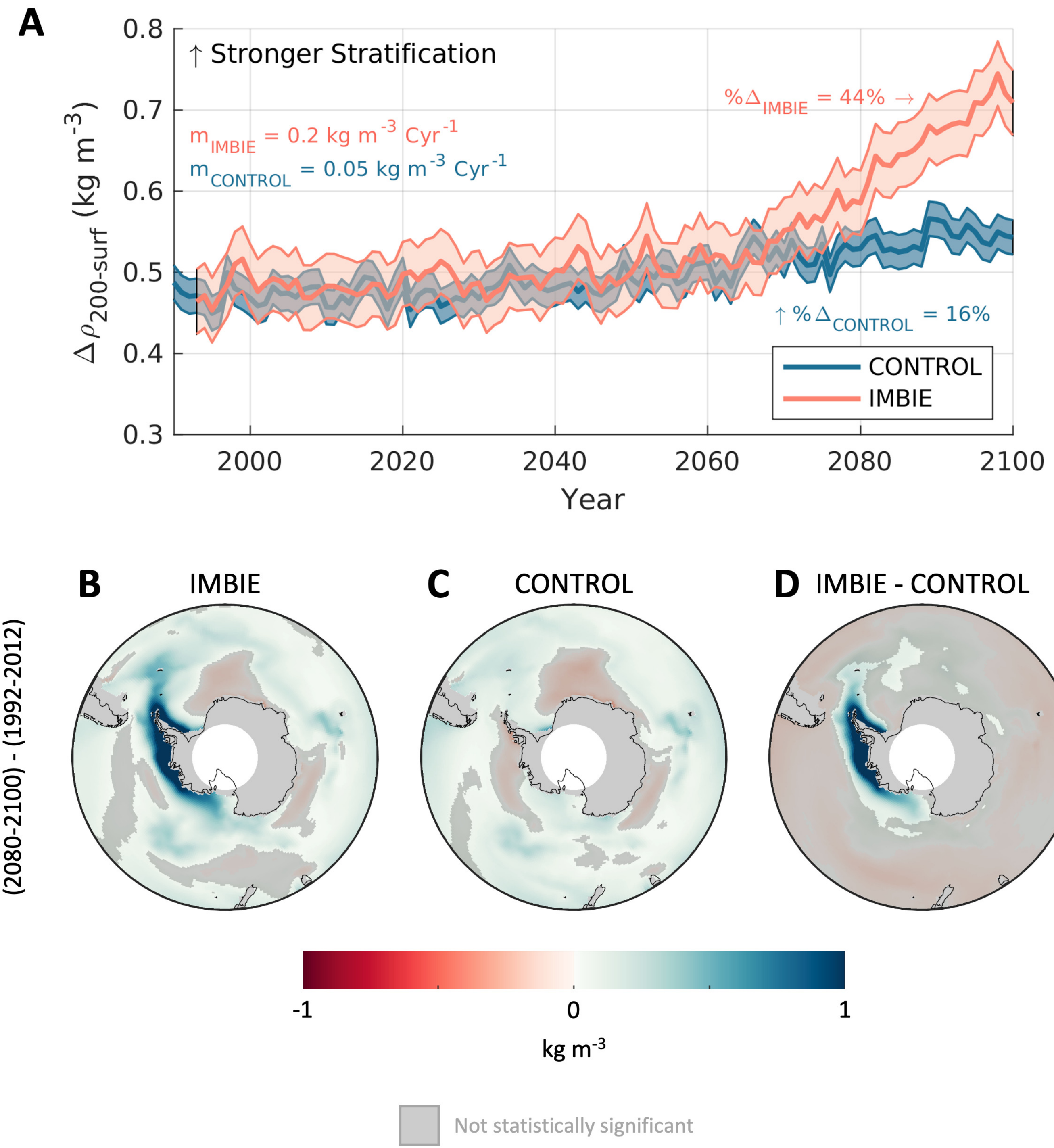
A
↑ Stronger Stratification
m_{IMBIE} = 0.2 kg m^{-3} Cyr^{-1}
$m_{CONTROL}$ = 0.05 kg m^{-3} Cyr^{-1}
%Δ_{IMBIE} = 44% →
↑ %$\Delta_{CONTROL}$ = 16%
CONTROL
IMBIE
$\Delta\rho_{200\text{-surf}}$ (kg m^{-3})
0.8
0.7
0.6
0.5
0.4
0.3
2000
2020
2040
2060
2080
2100
Year
B
IMBIE
C
CONTROL
D
IMBIE - CONTROL
(2080-2100) - (1992-2012)
-1
0
1
kg m^{-3}
Not statistically significant

Figure 2.

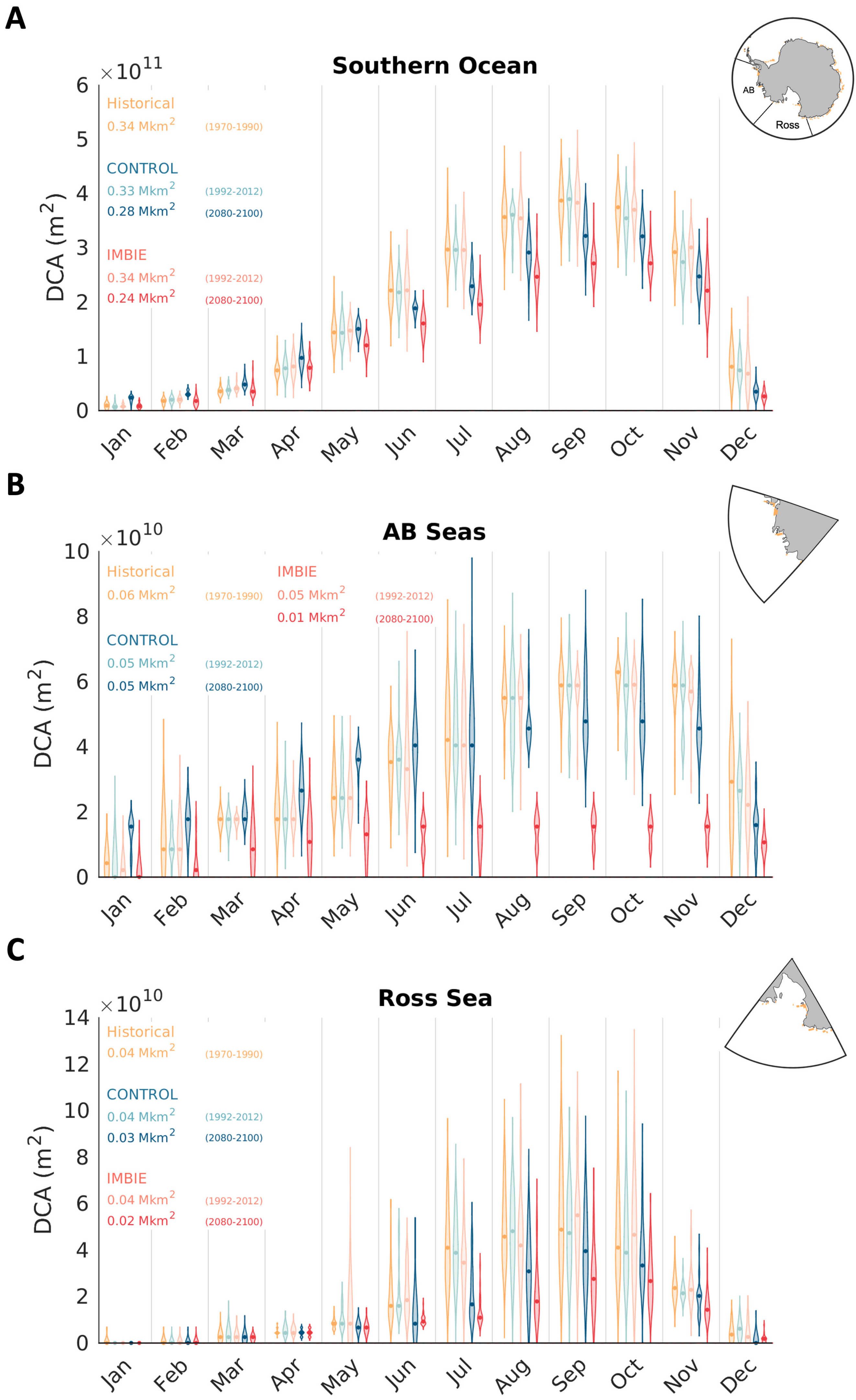

A
Southern Ocean
×10^11
Historical
0.34 Mkm² (1970-1990)
CONTROL
0.33 Mkm² (1992-2012)
0.28 Mkm² (2080-2100)
IMBIE
0.34 Mkm² (1992-2012)
0.24 Mkm² (2080-2100)
DCA (m²)
AB
Ross
Jan Feb Mar Apr May Jun Jul Aug Sep Oct Nov Dec
B
AB Seas
×10^10
Historical
0.06 Mkm² (1970-1990)
IMBIE
0.05 Mkm² (1992-2012)
0.01 Mkm² (2080-2100)
CONTROL
0.05 Mkm² (1992-2012)
0.05 Mkm² (2080-2100)
DCA (m²)
Jan Feb Mar Apr May Jun Jul Aug Sep Oct Nov Dec
C
Ross Sea
×10^10
Historical
0.04 Mkm² (1970-1990)
CONTROL
0.04 Mkm² (1992-2012)
0.03 Mkm² (2080-2100)
IMBIE
0.04 Mkm² (1992-2012)
0.02 Mkm² (2080-2100)
DCA (m²)
Jan Feb Mar Apr May Jun Jul Aug Sep Oct Nov Dec

Figure 3.

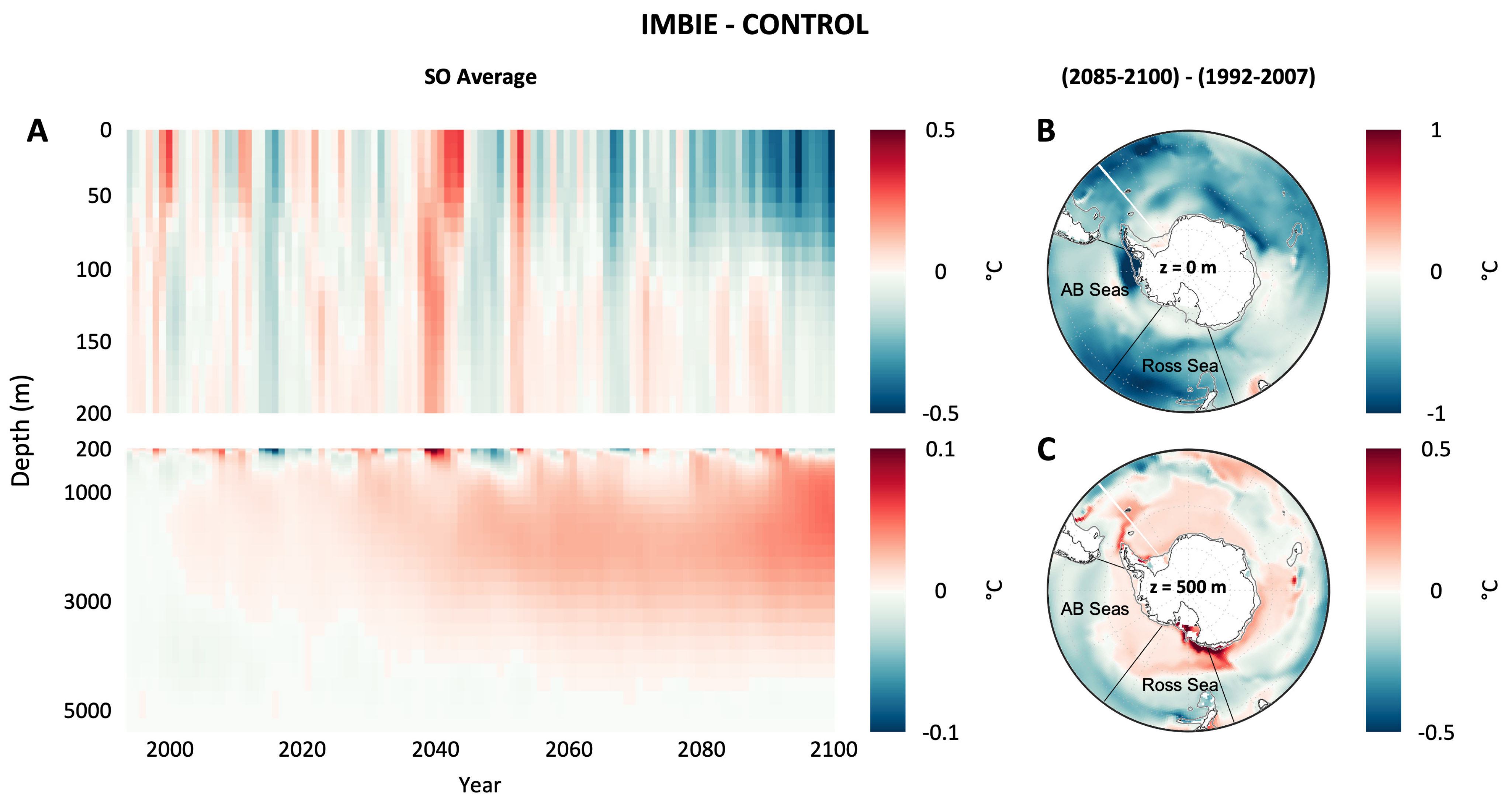

IMBIE - CONTROL
SO Average
(2085-2100) - (1992-2007)
A
B
C
Depth (m)
0
50
100
150
200
1000
3000
5000
2000
2020
2040
2060
2080
2100
Year
0.5
0
-0.5
0.1
-0.1
°C
1
-1
z = 0 m
z = 500 m
AB Seas
Ross Sea

Figure 4.

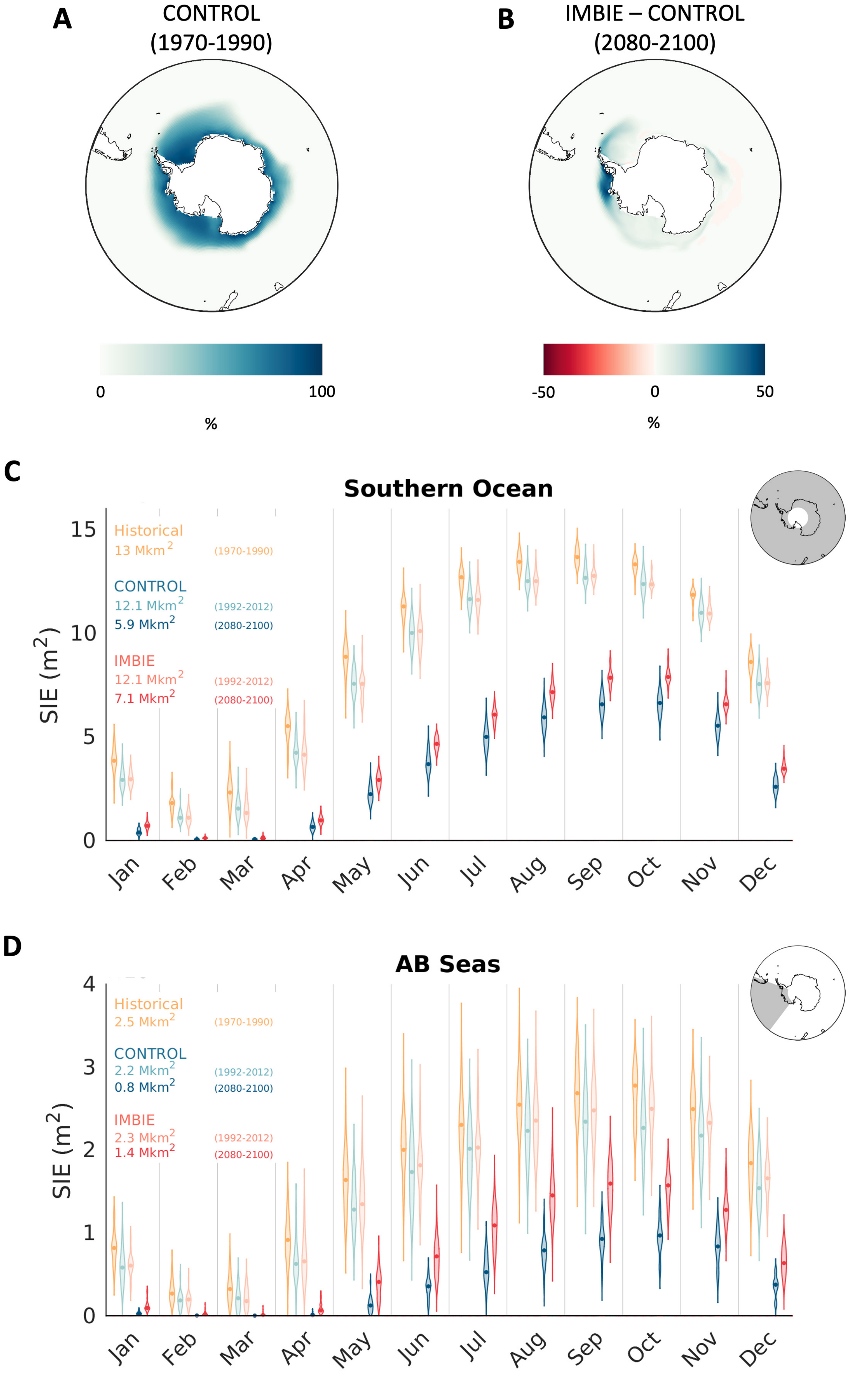
A
CONTROL
(1970-1990)
0
100
%
B
IMBIE – CONTROL
(2080-2100)
-50
0
50
%
C
Southern Ocean
Historical
13 Mkm²
(1970-1990)
CONTROL
12.1 Mkm²
(1992-2012)
5.9 Mkm²
(2080-2100)
IMBIE
12.1 Mkm²
(1992-2012)
7.1 Mkm²
(2080-2100)
SIE (m²)
Jan Feb Mar Apr May Jun Jul Aug Sep Oct Nov Dec
D
AB Seas
Historical
2.5 Mkm²
(1970-1990)
CONTROL
2.2 Mkm²
(1992-2012)
0.8 Mkm²
(2080-2100)
IMBIE
2.3 Mkm²
(1992-2012)
1.4 Mkm²
(2080-2100)
SIE (m²)
Jan Feb Mar Apr May Jun Jul Aug Sep Oct Nov Dec

Antarctic Ice Sheet freshwater discharge drives substantial Southern Ocean changes over the 21^{st} century

Tessa Gorte[1,2], Nicole Lovenduski[1,2], Cara Nisssen [1,2], Jan T. M. Lenaerts[1]

[1]Department of Atmospheric and Oceanic Sciences, University of Colorado Boulder, Boulder CO, USA
[2]Institute of Arctic and Alpine Research, University of Colorado Boulder, Boulder CO, USA

Key Points:

- We explore impacts of realistic Antarctic Ice Sheet (AIS) freshwater discharge on the Southern Ocean using a state-of-the-art climate model
- AIS discharge drives drastic changes in Southern Ocean stratification, winter deep convection, surface and interior temperature, and sea ice
- Our results suggest that regional AIS discharge can have far-reaching impacts on the Southern Ocean that can feedback on the climate system

Corresponding author: Tessa Gorte, `tessa.gorte@colorado.edu`

Abstract

Multidecadal satellite observations indicate that the Antarctic Ice Sheet (AIS) is losing mass at an accelerating rate, which has the potential to impact many aspects of the coupled climate system. While previous studies have demonstrated the importance of AIS freshwater discharge for regional and global climate processes using climate model experiments, many have applied unrealistic freshwater forcing. Here, we explore the potential Southern Ocean impacts of realistic AIS mass loss over the 21^{st} century in the Community Earth System Model version 2 (CESM2) by applying observation-based historical and ice sheet model-based future AIS freshwater forcing. The added freshwater reduces wintertime deep convective area by 72% while retaining 83% more sea ice. Congruent with other studies, we find the increased freshwater discharge extensively impacts local and remote Southern Ocean surface and subsurface temperature and stratification. These results demonstrate the necessity of accounting for AIS mass loss in global climate models for projecting future climate.

1 Introduction

Since the early 1990s, satellite-based observations have shown that the Antarctic Ice Sheet (AIS) is losing mass. The spatial pattern of AIS mass loss is heterogeneous (Rignot et al., 2019), mostly concentrated in the West Antarctic Ice Sheet (WAIS), which drains into the Amundsen and Bellingshausen Seas in the Southern Ocean (SO) (Velicogna & Wahr, 2006). The Ice sheet Mass Balance Inter-comparison Experiment version 2 (IMBIE2; Shepherd et al. (2018)) estimated that, from 1992-2017, the WAIS lost mass at a rate of 94 ± 27 Gt/y, and concluded that this mass loss has been accelerating (Rignot et al., 2019). Several studies using ice sheet models suggest that AIS mass loss will continue to accelerate in the future, as ice shelf thinning, grounding line retreat, and accelerating ice flow are all expected to continue and perhaps intensify with anthropogenic climate change(Pattyn & Morlighem, 2020; Gilbert & Kittel, 2021; Noble et al., 2020).

Apart from rising sea level (DeConto et al., 2021), AIS mass loss will affect many other aspects of the coupled climate system. Observations point to substantial physical changes in SO sea surface height, sea ice, water mass properties, and dense water formation, and a growing body of work attributes these changes to observed increases in AIS freshwater (FW) discharge (hereafter referred to as AIS discharge) (Jacobs & Giulivi, 2010; Fasullo & Nerem, 2018; Purich & England, 2023; Li et al., 2023). The SO's strong teleconnections to the global climate system mean that regional disruptions can precipitate broader changes elsewhere, across a range of timescales (Cabré & Gnanadesikan, 2017). Using climate model projections, previous work suggests that AIS FW fluxes will impact the future evolution of global atmospheric temperature and precipitation (Bronselaer et al., 2018), upper ocean stratification (Aiken & England, 2008; Swart & Fyfe, 2013), meridional overturning (Sadai et al., 2020; Moorman et al., 2020), and ocean temperature (Bintanja et al., 2015; Pauling et al., 2016; Park & Latif, 2019).

As AIS mass loss is not yet represented interactively in the latest generation of climate models, the potential impacts of AIS discharge on the coupled climate system are often investigated by directly applying anomalous FW fluxes to the ocean component of a climate model. Several studies apply FW forcing around AIS in a homogeneous fashion (Swart & Fyfe, 2013; Park & Latif, 2019; Purich & England, 2023) – inconsistent with the observed spatial pattern of AIS mass loss. Others aim to capture future melt of the large Ross and Ronne ice shelves, failing to reflect current grounded AIS mass loss (Bintanja et al., 2013, 2015). Pauling et al. (2016) explore potential impacts of spatially heterogeneous FW forcing but, like others (Aiken & England, 2008; Bintanja et al., 2013, 2015), impose FW abruptly with little to no gradual increase. Both Sadai et al. (2020) and Bronselaer et al. (2018) – which slowly increase the FW flux over several decades – employ global climate models (GCMs) from the Coupled Model Intercomparison Project version 5 (CMIP5) and apply a FW forcing based on CMIP5 Representative Concentration Pathway 8.5 (RCP8.5) runoff projections. These past studies have provided foundational understanding of the sensitivity of the climate system to large-scale AIS mass loss, but are unrealistic in representing the spatio-temporal variability in AIS mass changes and/or do not employ the latest versions of climate models (Landerer & Swenson, 2012).

Here, we apply a spatially heterogeneous FW signal that is reflective of the current spatial pattern of AIS mass loss that increases based on (1) satellite observations for the historical period and (2) CMIP6 Shared Socioeconomic Pathway 5-RCP8.5 (SSP5-8.5) runoff projections for the future period. Furthermore, we leverage the Community Earth System Model version 2 (CESM2), an Earth System Model from the updated suite of models in CMIP6. As we will demonstrate, the modeled Southern Ocean climate system is highly sensitive to AIS discharge – this discharge drives anomalous trends in vertical density stratification and surface and subsurface temperature as well as the seasonal cycles of sea ice and deep convective area. Furthermore, our results indicate that regional AIS discharge can impact these processes across the Southern Ocean basin.

2 Methods

In this paper, we run two fully coupled climate simulations using CESM2. CESM2 is a global climate model operated by the National Center for Atmospheric Research (NCAR), which we ran under historical CMIP6 greenhouse gas forcing from 1970-2015 and SSP5-8.5 greenhouse gas forcing from 2016-2100 with a $\sim 0.9 \times 1.25°$ horizontal resolution (Danabasoglu et al., 2020). The first simulation, CONTROL, runs from 1970-2100 with historical forcing through 2015 and SSP5-8.5 atmospheric forcing from 2016-2100. CESM2 preserves mass for the AIS via a mass threshold that, when exceeded, informs the model to transport excess mass to the nearest ocean grid cell as solid ice discharge. For our CONTROL simulation, we override this mechanism, and instead point the model to a prescribed runoff value of 2775 Gt y^{-1} (1 Gt = 1 Gigaton = 10^{12} kg) which is divided into six drainage basins with spatially variable FW discharge that is constant in time (Figure S1 illustrates the discharge from basal melt and calving assigned to each of the basins derived from Lenaerts et al. (2015)). The second simulation, IMBIE, branches off of the CONTROL simulation in 1992 and is run out to 2100 under the same forcing conditions. In the IMBIE simulation, AIS FW forcing initially has the same spatial pattern as the CONTROL but is allowed to change in time – we create a more realistic forcing that is observations-based for the historical period (1992-2020) and ice sheet modeling-based for the future period (2021-2100) (Rignot et al., 2019; DeConto & Pollard, 2016). For the observations-based forcing, we apply a linear fit to AIS mass balance data, amalgamated from various products by Rignot et al. (2019) such that FW discharge increases from 2775 in 1992 to $\sim$3160 Gt y^{-1} in 2020 (Figure S1). The future AIS FW forcing is based on output from DeConto et al. (2021) who use a combination of ice sheet and climate modeling to estimate the AIS contribution to global mean sea level out to 2300 under RCP8.5 atmospheric warming conditions. Their model output shows steady AIS mass balance through $\sim$2050 after which point, the AIS losses mass non-linearly. To reproduce their findings, our IMBIE FW forcing is constant in time from 2021-2050 and increases quasi-exponentially through 2100 ending at a value of 9280 Gt y^{-1} (Figure S1). Our AIS FW regime corresponds to a total AIS contribution to global mean sea level rise of just over 1 m by 2100. With observations currently indicating that the focus of AIS mass loss is in WAIS, we evenly distribute all of the additional AIS FW flux to the surface coastal grid cells in the co-located drainage basin in the Amundsen and Bellingshausen Seas (AB Seas; 95 °W to 145 °W) (Figure S1). We also subdivide our FW forcing into its solid (calving) and liquid (basal melt) components. Each basin has its own ratio of solid to liquid FW based on results from Depoorter et al. (2013) and these ratios are held constant for the entirety of the simulations (Figure S1). Over the AIS, calving and basal melt account for $\sim$48% and $\sim$52%, respectively.

For this paper, the SO is defined as the ocean south of 50 °S and we explore upper ocean stratification, deep convective area (DCA), surface and interior ocean temperature, and sea ice extent (SIE). We quantify upper ocean stratification as the difference of the potential density at 200 m and that at the surface ($\Delta\rho_{200-\mathrm{surf}} = \rho_{200} - \rho_{\mathrm{surf}}$) such that positive numbers correspond to higher densities at depth (i.e. stable stratification). DCA is calculated as the combined grid cell area under which the maximum mixed layer depth exceeds 50% of the bathymetry (Heuzé et al., 2013; Heuzé, 2021). As such, DCA is purely a metric for how well the water column is mixed. Its existence can be – but is not necessarily – related to the formation of precursors of Antarctic Bottom Water which ultimately depends on the density of the waters involved. CESM2 is one of the few CMIP6 models that accurately produces deep convection solely in the coastal regions (Heuzé, 2021). We define the surface ocean as the topmost vertical layer of the ocean model in CESM2 (10 m thick) and consider anything below the mixed layer (∼100-150 m) to be the interior ocean.

3 Results

4 Results

Meltwater changes the density structure of the SO, resulting in enhanced upper ocean stratification (Figure 1). The SO-averaged difference in stratification, $\Delta\rho_{200-\mathrm{surf}}$, increases for both simulations but significantly more so in the IMBIE simulation (1A). For the entire 1992-2100 simulation period, the IMBIE simulation $\Delta\rho_{200-\mathrm{surf}}$ increases by approximately 0.2 kg m^{-3} (44%) while the CONTROL simulation, by comparison, increases by 0.05 kg m^{-3} (16%). The difference in SO stratification between the two simulations is largely realized in the latter half of the 21st century with much of the increase in the IMBIE simulation occurring after 2070. The spatial realization of the enhanced stratification is such that the signal in the IMBIE is largely focused in the AB Seas region but also present in the Ross and Weddell Seas (Figure 1B-C). In these areas, the increase in stratification can be upwards of 1 kg m^{-3} which constitutes a first order of magnitude change on the historical mean state (Figure S1). Whereas, the CONTROL simulation shows no significant change in stratification over the course of the 21st century in these regions. Rather, the CONTROL simulation indicates a small increase in stratification in the open Southern Ocean, that is also captured in the IMBIE simulation (Figures 1B-C).

AIS discharge is associated with a significant reduction in Southern Ocean DCA (Figure 2). CESM2 develops deep convection in many Antarctic coastal regions in the historical simulation (Figure 2, yellow regions on map insets). Over the course of the century, both the CONTROL and IMBIE simulations project a decline in SO DCA from June through December, when DCA is at a maximum (Figure 2A). Austral winter DCA declines by 17% in the CONTROL simulation over the century, driven by anthropogenic changes other than AIS discharge (e.g., warming). Whereas, in the austral summer when the DCA is at a minimum, there is no statistically significant change in DCA over time or between simulations (Figure 2A). Including the effects of AIS discharge leads to a wintertime DCA reduction from a median value of 0.34 Mkm^2 to 0.24 Mkm^2; ∼29% (Figure 2A). Even with the 29% reduction in wintertime SO DCA in the IMBIE simulation, the median DCA for every month is within the extrema for the CONTROL(Figure 2A).

The AIS discharge-related reduction in SO DCA manifests most strongly in the AB Seas, where our model simulation projects a 75% decline in DCA in the austral winter months in the IMBIE simulation. Compared to a 13% decline in DCA for the CONTROL, this indicates substantially reduced seasonal DCA variability (Figure 2B). By the end of the century, the medians for the months of May as well as August through November are outside the extremes of the CONTROL DCA. The median CONTROL DCA in this region is also reduced from August-November but is within the historical DCA dis-

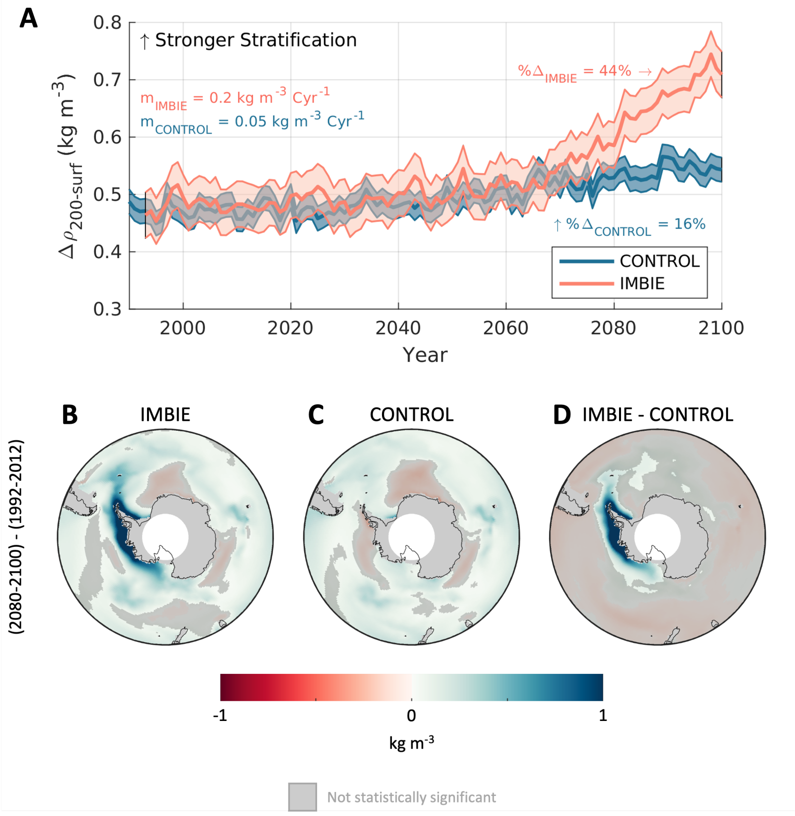

Figure 1. (A) Temporal evolution of the average SO potential density difference between the surface and 200 m depth ($\Delta\rho_{200-\mathrm{surf}}$) over 1990-2100 for both the CONTROL (blue) and IMBIE (peach) simulations. Larger numbers indicate stronger stratification. The solid line shows the SO average for each simulation and the shading indicates 1-σ. (B)-(C) End-of-century (2080-2100) minus beginning-of-century (1992-2012) $\Delta\rho_{200-\mathrm{surf}}$ in the IMBIE and CONTROL simulations, respectively. (D) Map of panel (B) - panel (C) showing the difference in the temporal evolution of stratification between the two simulations. Darker blues indicate stronger stratification with non-statistically significant changes shaded in grey.

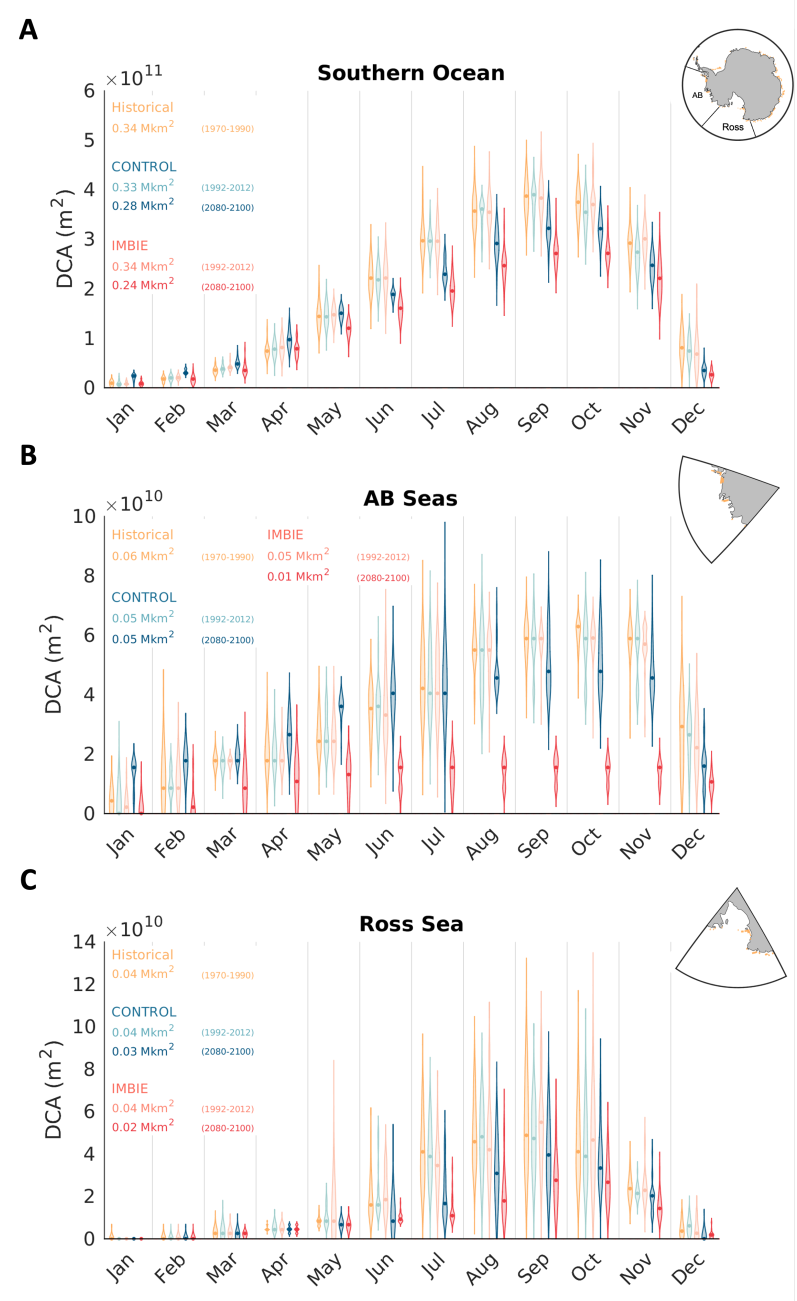

Figure 2. Monthly deep convective area climatology from the (yellow) 1970-1990 historical, (light blue) 1992-2012 CONTROL, (dark blue) 2080-2100 CONTROL, (peach) 1992-2012 IMBIE, and (red) 2080-2100 IMBIE periods/simulations averaged over the (A) Southern Ocean, (B) Amundsen/Bellingshausen Seas, and (C) Ross Sea regions. Maps in the upper right of each panel depict the region of interest as well as the historical DCA (yellow). The violin plots for each month represent the kernel density of DCA distribution. Each violin plot has a dot denoting the median DCA and the ends of the plot extend out to the extrema of the distribution.

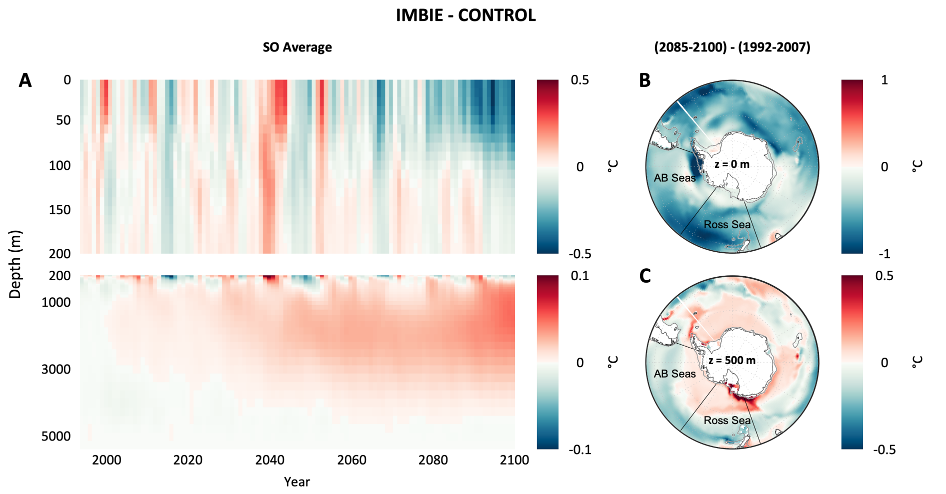

Figure 3. (A) The difference in average SO vertical temperature profile from 1992-2100 between the IMBIE and CONTROL simulations from 1992-2100. The upper panel depicts the top 200 m of the SO and has values ranging from -0.5 to 0.5 °C; the lower panel depicts 200 m to the ocean floor with values ranging from -0.1 to 0.1 °C. Bluer (redder) colors indicate when and at what depth the IMBIE simulation is cooler (warmer) than the CONTROL. (B) Difference (IMBIE-CONTROL) in SO surface temperature evolution comparing the 2080-2100 period to the 1992-2012 period. (C) Map of the difference (IMBIE-CONTROL) in SO 500 m depth temperature evolution comparing the 2080-2100 period to the 1992-2012 period. Black lines denote the boundaries of the AB Seas and Ross Sea regions.

tribution. The Ross Sea, whose DCA historically varies between ~0.04-0.1 Mkm^2 in the austral winter and spring shows a 52% reduction in DCA in the IMBIE simulation and a 30% reduction in the CONTROL from July-November. The median IMBIE DCA is within the broad (and thus highly variable) historical distribution of DCA for the Ross Sea. As such, our simulations indicate that AIS discharge reduces deep convection both regionally in the AB Seas as well as in regions outside of where the FW forcing is applied, such as the Ross Sea.

AIS discharge leads to anomalous cooling in the surface and anomalous warming in the subsurface of the SO. The surface and subsurface SO warm ubiquitously in both simulations with anthropogenic climate change (Figure S3). The surface SO warms 0.28 °C less in the IMBIE simulation than in the CONTROL by 2100 (1.8 and 1.5 °C respectively). This anomalous cooling, which extends through the mixed layer (~100 m), begins to appear mid-century, and intensifies after ~2070 (Figure 3A). Anomalous surface ocean cooling in response to AIS discharge manifests most strongly in the AB Seas region, where we impose the strongest FW forcing (Figure 3B; Figure S1). Here, surface temperatures from the IMBIE simulation are nearly 2 °C cooler than those in the CONTROL simulation. Another area of anomalous cooling due to FW input manifests off the coast of the East AIS near Enderby Land; a region of low SIE.

In contrast to the surface cooling, the deep SO (500 - 3000 m) experiences anomalous warming with AIS discharge over the course of the century. Averaged over the SO, the IMBIE simulation warms by 0.70 °C compared to 0.63 °C in the CONTROL. As such, the IMBIE simulation is 0.07 °C warmer than the CONTROL on average between 500-3000 m depth by the end of the century (Figure 3A). The anomalous warming of the deep Southern Ocean is spatially heterogeneous. Figure 3C shows anomalously warm temperatures (~0.01 °C) extending from the coast northward to the core of the Antarctic Circumpolar Current, with much larger anomalies (0.89°C) in the Ross Sea and along the Adélie Coast at 500m. Notably, this pocket of anomalously warm water is not co-located with the AIS FW input.

Both simulations show an overall loss of sea ice over the 21^{st} century with anthropogenic climate change, however, the IMBIE simulation shows significantly less extensive sea ice loss, especially in the austral winter/spring (July-November). The historical SO sea ice cover is largely circumpolar with the highest concentrations in the Weddell and Ross Seas (Figure 4A). By the end of the century (2080-2100) the IMBIE simulation retains over 50% more sea ice in the AB Seas region (Figure 4B). The Weddell and Ross Seas – particularly out at the sea ice edge near the peninsula – also preserve over 25% more sea ice than the CONTROL (Figure 4B). Historical SIE typically reaches an annual maximum in September-October and an annual minimum between February-March and can vary between 2-15 Mkm^2, seasonally, across the entire SO (Figure 4D). In the AB Seas, SIE varies between 0.25-3.25 Mkm^2. For both the AB Seas as well as the entire SO, there is a significant decline in SIE from the 1992-2012 period to the 2080-2100 period, driven by anthropogenic climate change (Figure 4C-D). However, there is a significant difference in SIE between the IMBIE and CONTROL simulations by the end of the century, particularly in the austral winter and spring (Figure 4C-D). For five months out of the year, the IMBIE simulation produces over 1 Mkm^2 more total SO sea ice than the CONTROL in the 2080-2100 period with the maximum, 1.3 Mkm^2 in September, equivalent to ~9% of the total historical SIE (Figure 4C). This disparity in SIE is largely due to more sea ice preservation in the AB Seas region, which retains nearly 20% more sea ice in the IMBIE simulation compared to the CONTROL (Figure 4D).

5 Conclusions and Discussion

To investigate the potential role of projected AIS discharge on the SO, we conducted analysis using two fully coupled climate simulations with identical atmospheric forcing but different AIS FW fluxes. AIS discharge anomalously increases upper ocean stratification by ~30% across the Southern Ocean, with large increases in the AB Seas, and smaller increases in the Weddell and Ross Seas. End-of century Southern Ocean wintertime deep convective area is 0.34 Mkm^2 in the control simulation, but only 0.24 Mkm^2 in the IMBIE simulation. Regionally, we see the strongest impacts in the AB Seas region as wintertime DCA is reduced to summertime levels while DCA in the Ross Sea declines by ~22% due to the FW. The IMBIE surface ocean is 0.28 °C cooler than that of the CONTROL while the subsurface warms significantly with warmer regions focused in the western Ross Sea and along the Adélie Land coast. Our simulations also project that the freshening and anomalous cooling of the surface SO induce conditions more favorable for sea ice formation.

Our results suggest that the freshening of the AB seas, and to a lesser extent, the broader Southern Ocean, is the primary driver of the enhanced stratification in the IMBIE simulation. Surface temperature cools while subsurface temperature warms in response to AIS discharge, a change that would induce reduced stratification if no salinity anomalies were present. The freshening and anomalous cooling of the surface SO induce conditions more favorable for sea ice formation. Previous studies have noted the importance of the ice-albedo feedback wherein when sea ice melts, it exposes the darker surface ocean below, lowering the albedo, increasing ocean heat uptake, inducing more sea ice melt and/or less sea ice growth (Curry et al., 1995). With the IMBIE simulation preserving more sea ice than the CONTROL, this positive feedback loop is suppressed, and the surface ocean is relatively cooler. When sea ice forms, however, it releases heat and rejects the oceanic brine, increasing the surface temperature and salinity, and thus inducing a negative feedback loop. The lower surface temperature and salinity in the IM-

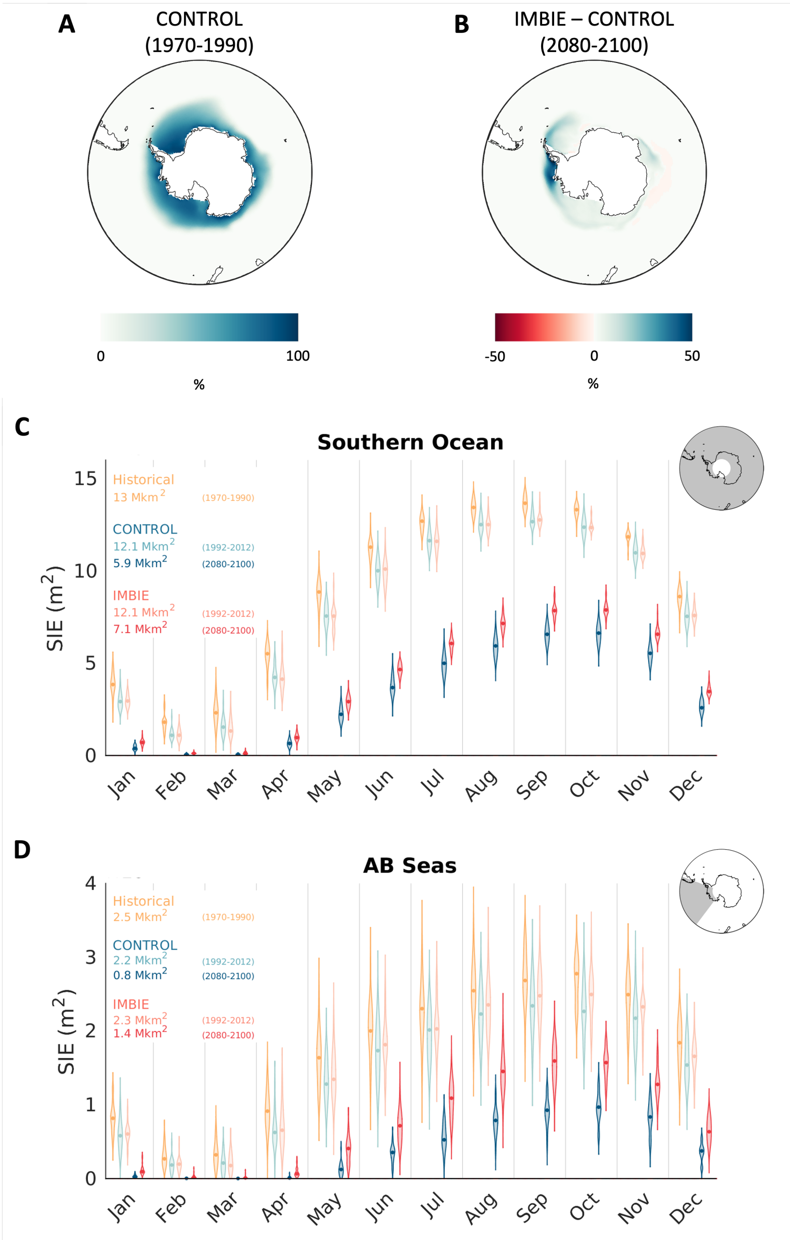

Figure 4. (A) Average annual mean of SIF in each grid cell for the 1970-1990 historical period. (B) the average difference in SIF between the IMBIE and CONTROL simulations during the 2080-2100 period. (C) Monthly SIE for the whole SO in the historical (yellow), 1992-2012 CONTROL (light blue), 2080-2100 CONTROL (dark blue), 1992-2012 IMBIE (peach), and 2080-2100 IMBIE (red) periods. The violin plots for each month represent the kernel density of SIE distribution. Each violin plot has a dot denoting the median SIE and the ends of the plot extend out to the extrema of the distribution.

BIE simulation, then, implies that the heat uptake (or lack thereof) and the FW discharge dominate the sea ice formation signal for the evolution of both variables. FW-induced changes to stratification and DCA as well as surface and interior temperature all permeate into more remote regions of the SO, mainly the Ross and Weddell Seas. Deep convection, which only occurs in coastal grid cells, is most strongly affected in the AB Seas but also manifests remotely in the Ross Sea. The loss in DCA is realized predominantly from July-November such that the historical wintertime high is reduced to summertime low levels in the AB Seas. This period aligns with that of the highest sea ice retention – most of the preserved sea ice exists in the AB Seas and, to a lesser extent, the Ross and Weddell Seas.

Our findings are supported by those reported in other studies. Compared to Bronselaer et al. (2018), Sadai et al. (2020), and Purich and England (2023), our SIE and surface and interior temperature manifest similarly in strength and spatial pattern with much of the AB Seas sea ice persisting despite strong anthropogenic warming and anomalous warming of the western Ross Sea. We find the sea ice response to be significantly less than what was found in the ice-shelf specific sensitivity experiments of Bintanja et al. (2013) and Bintanja et al. (2015). While we do see a differential sea ice response by the end of the century, the FW-induced changes are not statistically significantly different until after 2070; nearly 80 years into the simulation. As such, we find the minimal sea ice response in extent and trend over <50 model years as seen by Swart and Fyfe (2013) and Pauling et al. (2016), respectively, to be consistent with our results. Bintanja et al. (2013) find that the strength of their FW forcing engenders a sea ice response strong enough to account for the disparate observed SO sea ice cover. Our historical SO sea ice cover, which peaks at $\sim$15 Mkm^2 in September, is already lower than the observed 18-20 Mkm^2 in September SIE. Likely owing to anthropogenic warming, there is a significant overall reduction in SO SIE on the order of $\sim$5-8 Mkm^2 with the IMBIE simulation retaining $\sim$1 Mkm^2 more than the CONTROL by the end of the century. That is to say, the FW discharge does help preserve SO SIE but not enough to offset anthropogenic warming. Like Park and Latif (2019) and Li et al. (2023), we also see a decline in deep convection in the SO; both of which use models noted for producing too much open ocean deep convection (Heuzé, 2021).

There are three major caveats with this work: (1) the assumption that past observations are a good predictor of future changes, (2) the assumption of ice shelf mass (im)balance, and (3) the application of our FW forcing. We assume that past AIS melt patterns will continue into the future. Our understanding of the decades-to-centuries long spatio-temporal changes to AIS mass balance is limited, as mass change records from the GRACE satellite missions are only 20 years long. Ice sheet models – which are informed by these and other observations – project sustained elevated mass loss in the West AIS region over the course of the next century (DeConto & Pollard, 2016). Further, the GRACE satellites only measure the mass balance of the grounded ice sheet, not the ice shelves, leaving us with little information about large-scale ice shelf mass (im)balances across the AIS. In addition, CESM2 cannot model floating ice shelves. As such, we assume that the AIS ice shelves are in mass balance and that continental mass changes are directly realized as FW fluxes. These FW fluxes, then, are introduced solely to the coastal surface grid cells, though previous work indicates that similar GCMs are sensitive to neither the horizontal FW distribution close to or far from the coast nor the vertical FW distribution meaning our FW flux spatial distribution is reasonable for this assessment Bronselaer et al. (2018); Pauling et al. (2016). Finally, we leverage observed AIS mass changes from the GRACE satellites to guide historical (1992-2020) FW discharge and GCM output for future (2021-2100) discharge. The GCM (CESM1) projection we use for future AIS mass balance is (1) based on a model that doesn't have an active ice sheet and, thus, inherently misses any feedbacks with the coupled climate system and (2) generally constant until about 2050, after which point, it increases dramatically (DeConto et al., 2021).

Stitching these two forcings together, then, means that from 2021-2050, there is a constant annual FW forcing from the AIS that is guided by limited information.

Our results nevertheless demonstrate the potential ramifications of AIS FW discharge on the climate system. AIS FW is likely to play a key role in the spatio-temporal evolution of the SO over the 21^{st} century. Given the importance of the SO for the uptake of anthropogenic heat and carbon (Frölicher et al., 2015), it is reasonable to expect that AIS FW discharge will engender climate feedbacks in the coming century and beyond.

6 Open Research

Data from the CONTROL simulation presented in this paper are publicly available at https://doi.org/10.5281/zenodo.8056558 (Gorte et al., 2023a). Data from the IMBIE simulation presented in this paper are publicly available at https://doi.org/10.5281/zenodo.8058223 (Gorte et al., 2023b).

Acknowledgments

We would like to thank Dr. Leo van Kampenhout for his work in the setup of these experiments.

This work was performed at the University of Colorado Boulder and Institute of Arctic and Alpine Research and was supported by the NASA's Sea Level Change Team (award #80NSSC20K1123). We would also like to acknowledge NCAR's Land Ice and Polar Climate Working Groups for their valuable computing time contributions.

References

Aiken, C. M., & England, M. H. (2008, 8). Sensitivity of the present-day climate to freshwater forcing associated with antarctic sea ice loss. *Journal of Climate*, *21*, 3936-3946. doi: 10.1175/2007JCLI1901.1

Bintanja, R., Oldenborgh, G. J. V., Drijfhout, S. S., Wouters, B., & Katsman, C. A. (2013, 5). Important role for ocean warming and increased ice-shelf melt in antarctic sea-ice expansion. *Nature Geoscience*, *6*, 376-379. doi: 10.1038/NGEO1767

Bintanja, R., Oldenborgh, G. J. V., & Katsman, C. A. (2015). The effect of increased fresh water from antarctic ice shelves on future trends in antarctic sea ice. *Annals of Glaciology*, *56*, 120-126. doi: 10.3189/2015AOG69A001

Bronselaer, B., Winton, M., Griffies, S. M., Hurlin, W. J., Rodgers, K. B., Sergienko, O. V., ... Russell, J. L. (2018, 11). Change in future climate due to antarctic meltwater. *Nature 2018 564:7734*, *564*, 53-58. Retrieved from `https://www.nature.com/articles/s41586-018-0712-z` doi: 10.1038/s41586-018-0712-z

Cabré, A., & Gnanadesikan, A. (2017). Global atmospheric teleconnections and multidecadal climate oscillations driven by southern ocean convection. Retrieved from `www.ametsoc.org/PUBSReuseLicenses` doi: 10.1175/JCLI-D-16-0741.s1

Curry, J. A., Schramm, J. L., & Ebert, E. E. (1995). Sea ice-albedo climate feedback mechanism. *Journal of Climate*, *8*, 240 - 247. Retrieved from `https://journals.ametsoc.org/view/journals/clim/8/2/1520-0442_1995_008_0240_siacfm_2_0_co_2.xml` doi: https://doi.org/10.1175/1520-0442(1995)008⟨0240:SIACFM⟩2.0.CO;2

Danabasoglu, G., Lamarque, J. F., Bacmeister, J., Bailey, D. A., DuVivier, A. K., Edwards, J., ... Strand, W. G. (2020, 2). The community earth system model version 2 (cesm2). *Journal of Advances in Modeling Earth Systems*, *12*, e2019MS001916. Retrieved from https://onlinelibrary.wiley.com/doi/full/10.1029/2019MS001916https://onlinelibrary.wiley.com/doi/abs/10.1029/2019MS001916https://agupubs.onlinelibrary.wiley.com/doi/10.1029/2019MS001916 doi: 10.1029/2019MS001916

DeConto, R. M., & Pollard, D. (2016, 3). Contribution of antarctica to past and future sea-level rise. *Nature*, *531*, 591-597. doi: 10.1038/nature17145

DeConto, R. M., Pollard, D., Alley, R. B., Velicogna, I., Gasson, E., Gomez, N., ... Dutton, A. (2021, 5). The paris climate agreement and future sea-level rise from antarctica. *Nature 2021 593:7857*, *593*, 83-89. Retrieved from https://www.nature.com/articles/s41586-021-03427-0 doi: 10.1038/s41586-021-03427-0

Depoorter, M. A., Bamber, J. L., Griggs, J. A., Lenaerts, J. T., Ligtenberg, S. R., Broeke, M. R. V. D., & Moholdt, G. (2013). Calving fluxes and basal melt rates of antarctic ice shelves. *Nature*, *502*, 89-92. doi: 10.1038/nature12567

Fasullo, J. T., & Nerem, R. S. (2018, 12). Altimeter-era emergence of the patterns of forced sea-level rise in climate models and implications for the future. *Proceedings of the National Academy of Sciences of the United States of America*, *115*, 12944-12949. doi: 10.1073/pnas.1813233115

Frölicher, T. L., Sarmiento, J. L., Paynter, D. J., Dunne, J. P., Krasting, J. P., & Winton, M. (2015). Dominance of the southern ocean in anthropogenic carbon and heat uptake in cmip5 models. *Journal of Climate*, *28*, 862-886. doi: 10.1175/JCLI-D-14-00117.1

Gilbert, E., & Kittel, C. (2021, 4). Surface melt and runoff on antarctic ice shelves at 1.5°c, 2°c, and 4°c of future warming. *Geophysical Research Letters*, *48*, e2020GL091733. Retrieved from https://onlinelibrary.wiley.com/doi/full/10.1029/2020GL091733https://onlinelibrary.wiley.com/doi/abs/10.1029/2020GL091733https://agupubs.onlinelibrary.wiley.com/doi/10.1029/2020GL091733 doi: 10.1029/2020GL091733

Gorte, T., Lovenduski, N., Nissen, C., & Lenaerts, J. T. (2023a, June). *CESM2 CONTROL simulation output: Antarctic Ice Sheet freshwater discharge drives substantial Southern Ocean changes over the 21st century.* Zenodo. Retrieved from https://doi.org/10.5281/zenodo.8056558 doi: 10.5281/zenodo.8056558

Gorte, T., Lovenduski, N., Nissen, C., & Lenaerts, J. T. (2023b, June). *CESM2 IMBIE simulation output: Antarctic Ice Sheet freshwater discharge drives substantial Southern Ocean changes over the 21st century.* Zenodo. Retrieved from https://doi.org/10.5281/zenodo.8058223 doi: 10.5281/zenodo.8058223

Heuzé, C. (2021, 1). Antarctic bottom water and north atlantic deep water in cmip6 models. *Ocean Science*, *17*, 59-90. doi: 10.5194/os-17-59-2021

Heuzé, C., Heywood, K. J., Stevens, D. P., & Ridley, J. K. (2013, 4). Southern ocean bottom water characteristics in cmip5 models. *Geophysical Research Letters*, *40*, 1409-1414. doi: 10.1002/grl.50287

Jacobs, S. S., & Giulivi, C. F. (2010, 9). Large multidecadal salinity trends near the pacific-antarctic continental margin. *Journal of Climate*, *23*, 4508-4524. doi: 10.1175/2010JCLI3284.1

Landerer, F. W., & Swenson, S. C. (2012). Accuracy of scaled grace terrestrial water storage estimates. *Water Resources Research*, *48*. doi: 10.1029/2011WR011453

Lenaerts, J. T. M., Bars, D. L., van Kampenhout, L., Vizcaino, M., Enderlin, E. M., & van den Broeke, M. R. (2015, 8). Representing greenland ice sheet freshwater fluxes in climate models. *Geophysical Research Letters*, *42*, 6373-6381. Retrieved from http://doi.wiley.com/10.1002/2015GL064738 doi: 10.1002/2015GL064738

Li, Q., England, M. H., Hogg, A. M., Rintoul, S. R., & Morrison, A. K. (2023, 3). Abyssal ocean overturning slowdown and warming driven by antarctic meltwater. *Nature*, *615*, 841-847. Retrieved from https://www.nature.com/articles/s41586-023-05762-w doi: 10.1038/s41586-023-05762-w

Moorman, R., Morrison, A. K., & Hogg, A. M. C. (2020, 8). Thermal responses to antarctic ice shelf melt in an eddy-rich global ocean-sea ice model. *Journal of Climate*, *33*, 6599-6620. doi: 10.1175/JCLI-D-19-0846.1

Noble, T. L., Rohling, E. J., Aitken, A. R., Bostock, H. C., Chase, Z., Gomez, N., ... Williams, T. (2020, 12). The sensitivity of the antarctic ice sheet to a changing climate: Past, present, and future. *Reviews of Geophysics*, *58*, e2019RG000663. Retrieved from https://onlinelibrary.wiley.com/doi/full/10.1029/2019RG000663https://onlinelibrary.wiley.com/doi/abs/10.1029/2019RG000663https://agupubs.onlinelibrary.wiley.com/doi/10.1029/2019RG000663 doi: 10.1029/2019RG000663

Park, W., & Latif, M. (2019, 3). Ensemble global warming simulations with idealized antarctic meltwater input. *Climate Dynamics*, *52*, 3223-3239. doi: 10.1007/s00382-018-4319-8

Pattyn, F., & Morlighem, M. (2020, 3). The uncertain future of the antarctic ice sheet. *Science*, *367*, 1331-1335. Retrieved from https://www.science.org/doi/10.1126/science.aaz5487 doi: 10.1126/SCIENCE.AAZ5487/ASSET/D0DE1D3F-7990-45CB-9D79-D9B922FD6075/ASSETS/GRAPHIC/367_1331_F4.JPEG

Pauling, A. G., Bitz, C. M., Smith, I. J., & Langhorne, P. J. (2016). The response of the southern ocean and antarctic sea ice to freshwater from ice shelves in an earth system model. *Journal of Climate*, *29*, 1655-1672. doi: 10.1175/JCLI-D-15-0501.1

Purich, A., & England, M. H. (2023, 1). Projected impacts of antarctic meltwater anomalies over the twenty-first century. *Journal of Climate*, *36*, 2703-2719. doi: 10.1175/jcli-d-22-0457.1

Rignot, E., Mouginot, J., Scheuchl, B., van den Broeke, M., van Wessem, M. J., & Morlighem, M. (2019). Four decades of antarctic ice sheet mass balance from 1979–2017. *Proceedings of the National Academy of Sciences*, *116*, 1095-1103. doi: 10.1073/pnas.1812883116

Sadai, S., Condron, A., DeConto, R., & Pollard, D. (2020, 9). Future climate response to antarctic ice sheet melt caused by anthropogenic warming. *Science Advances*, *6*, eaaz1169. Retrieved from http://advances.sciencemag.org/ doi: 10.1126/sciadv.aaz1169

Shepherd, A., Ivins, E., Rignot, E., Smith, B., Broeke, M. V. D., Velicogna, I., ... Wouters, B. (2018, 6). *Mass balance of the antarctic ice sheet from 1992 to 2017* (Vol. 558). Nature Publishing Group. doi: 10.1038/s41586-018-0179-y

Swart, N. C., & Fyfe, J. C. (2013, 8). The influence of recent antarctic ice sheet retreat on simulated sea ice area trends. *Geophysical Research Letters*, *40*, 4328-4332. doi: 10.1002/GRL.50820

Velicogna, I., & Wahr, J. (2006, 3). Measurements of time-variable gravity show mass loss in antarctica. *Science*, *311*, 1754-1756. Retrieved from https://www.science.org/doi/10.1126/science.1123785 doi: 10.1126/SCIENCE.1123785/ASSET/930F3A74-2360-4753-ADB9-8ED78286A1F8/ASSETS/GRAPHIC/311_1754_F3.JPEG

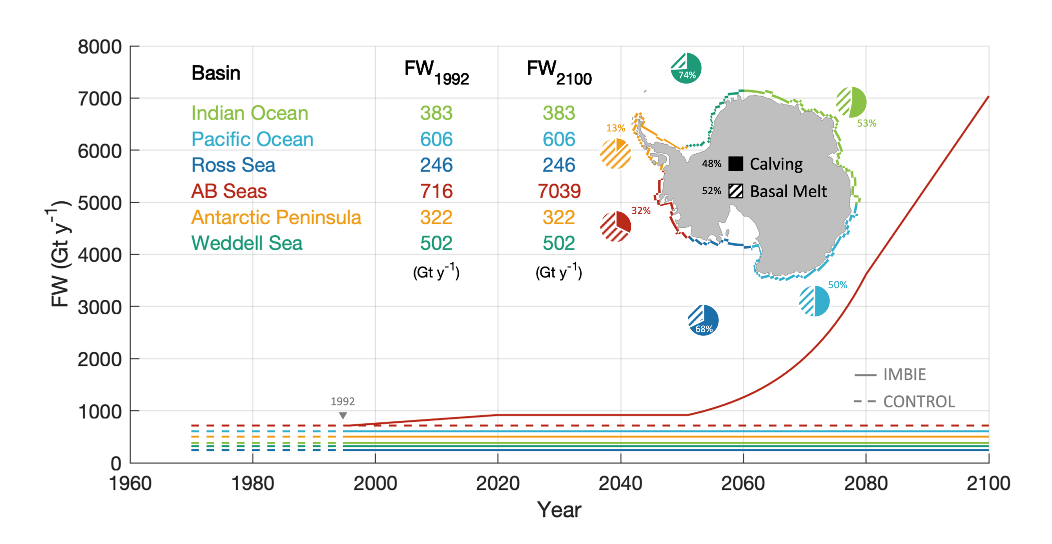

Figure S1. The AIS FW distribution shown spatially and as a time series. The 6 basins we define are the Weddell Sea (dark green), the Indian Ocean (light green), the Pacific Ocean (light blue), the Ross Sea (dark blue), the AB Seas (red), and the Antarctic Peninsula (orange). Each basin has its own ratio of calving to basal melt as depicted by the pie charts (percentages denote the percent of FW flux realized as calving). The time series show the total FW fluxing from each basin for the CONTROL (dashed) and the IMBIE (solid) simulations; the latter of which branches off in 1992. Also displayed are the values of total FW fluxing from each basin in 1992 and in 2100 in Gt y^{-1}.

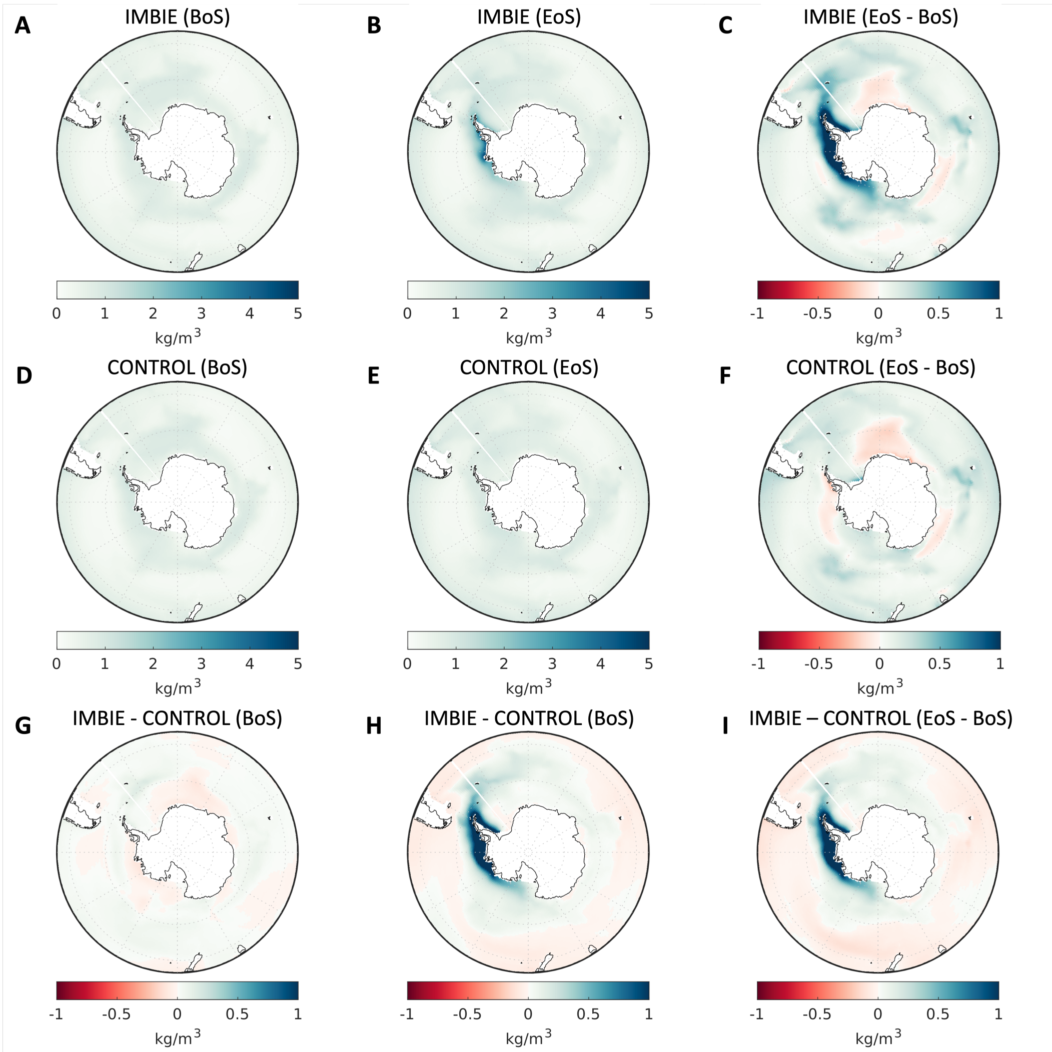

Figure S2. Snapshots of density stratification (200 m - surface) for the IMBIE simulation (top row), CONTROL simulation (middle row), and the difference (IMBIE - CONTROL; bottom row). The columns depict the average stratification for the periods of 1992-2007 (left), 2085-2100 (center), and the difference (right).

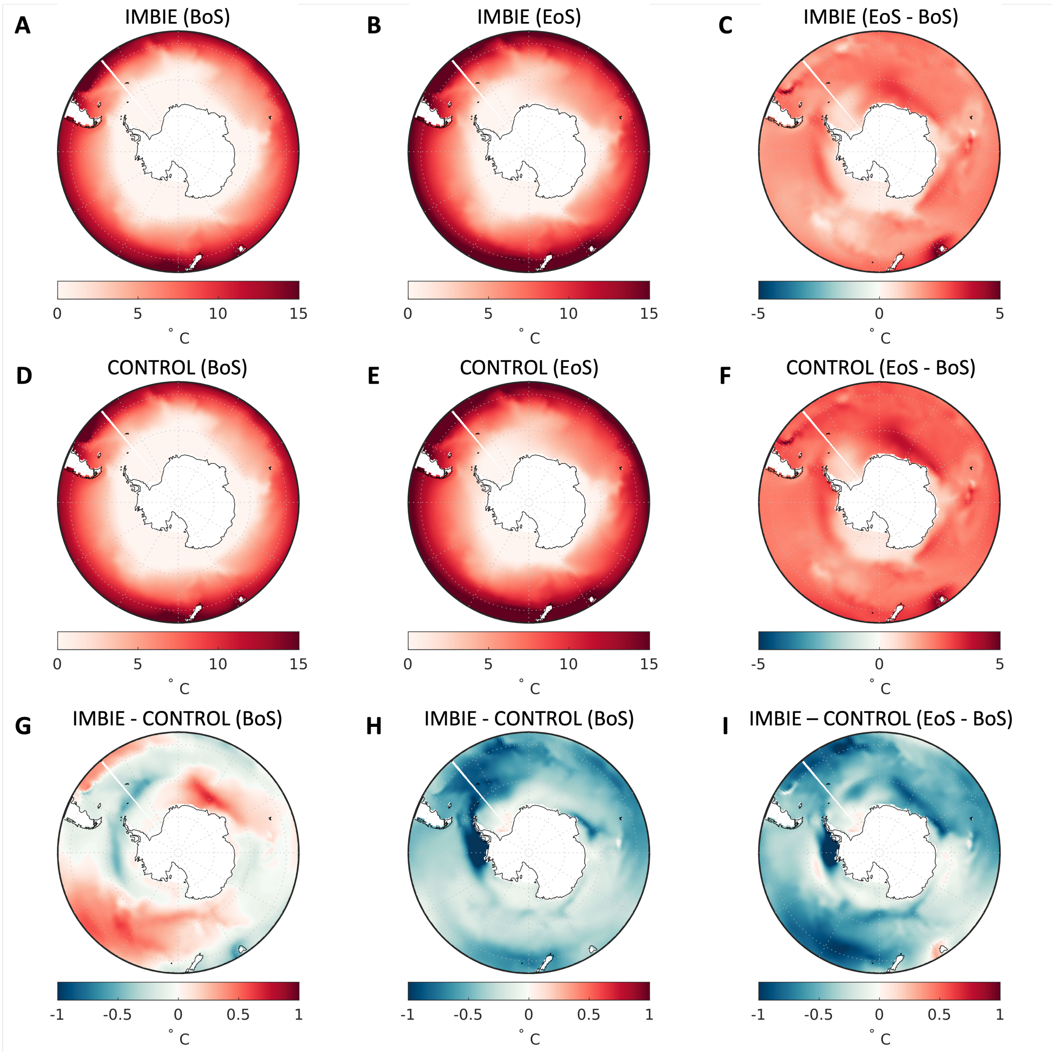

Figure S3. Snapshots of surface temperature for the IMBIE simulation (top row), CONTROL simulation (middle row), and the difference (IMBIE - CONTROL; bottom row). The columns depict the average surface temperature for the beginning of the simulation (BoS) from 1992-2007 (left), the end of the simulation (EoS) 2085-2100 (center), and the difference (right).

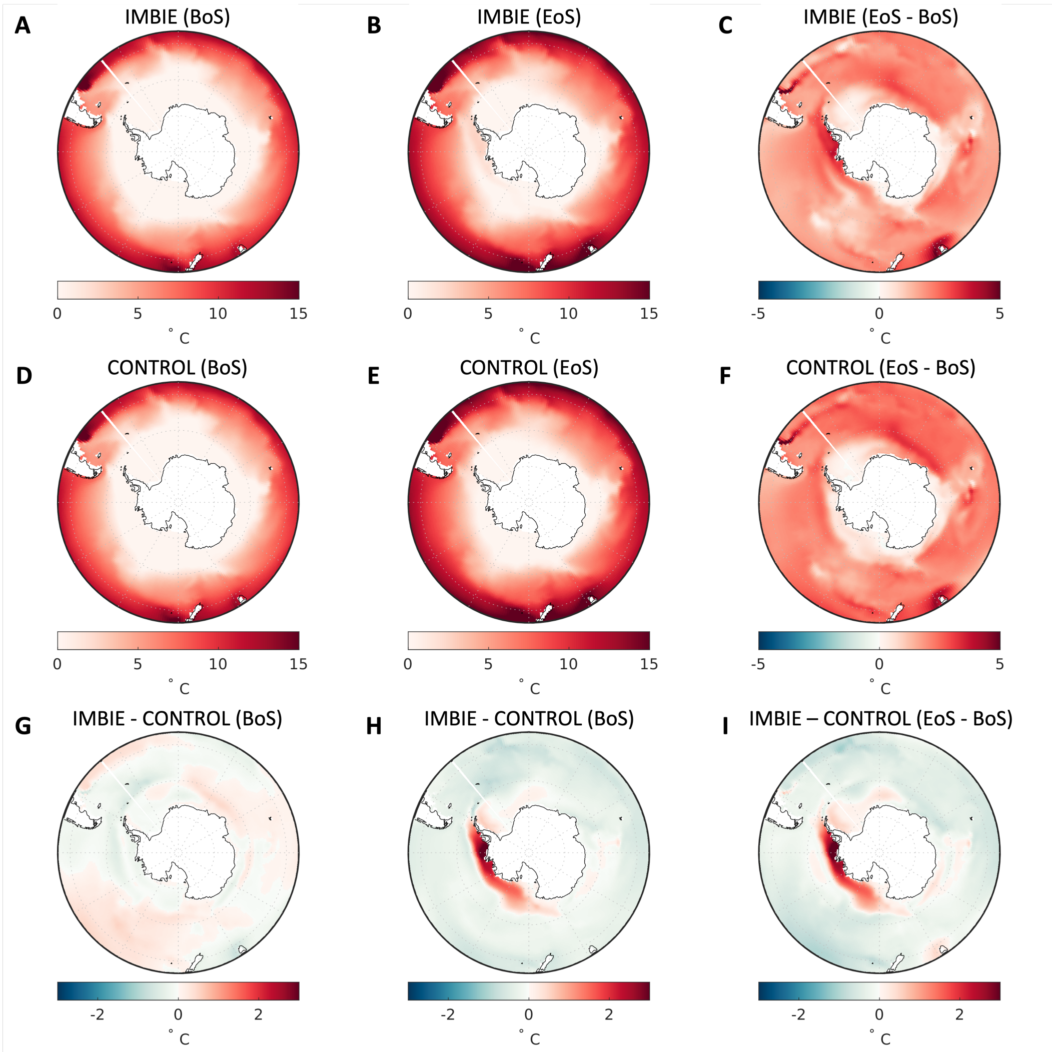

Figure S4. Snapshots of T_{100} for the IMBIE simulation (top row), CONTROL simulation (middle row), and the difference (IMBIE - CONTROL; bottom row). The columns depict the average T_{100} for the beginning of the simulation (BoS) from 1992-2007 (left), the end of the simulation (EoS) 2085-2100 (center), and the difference (right).

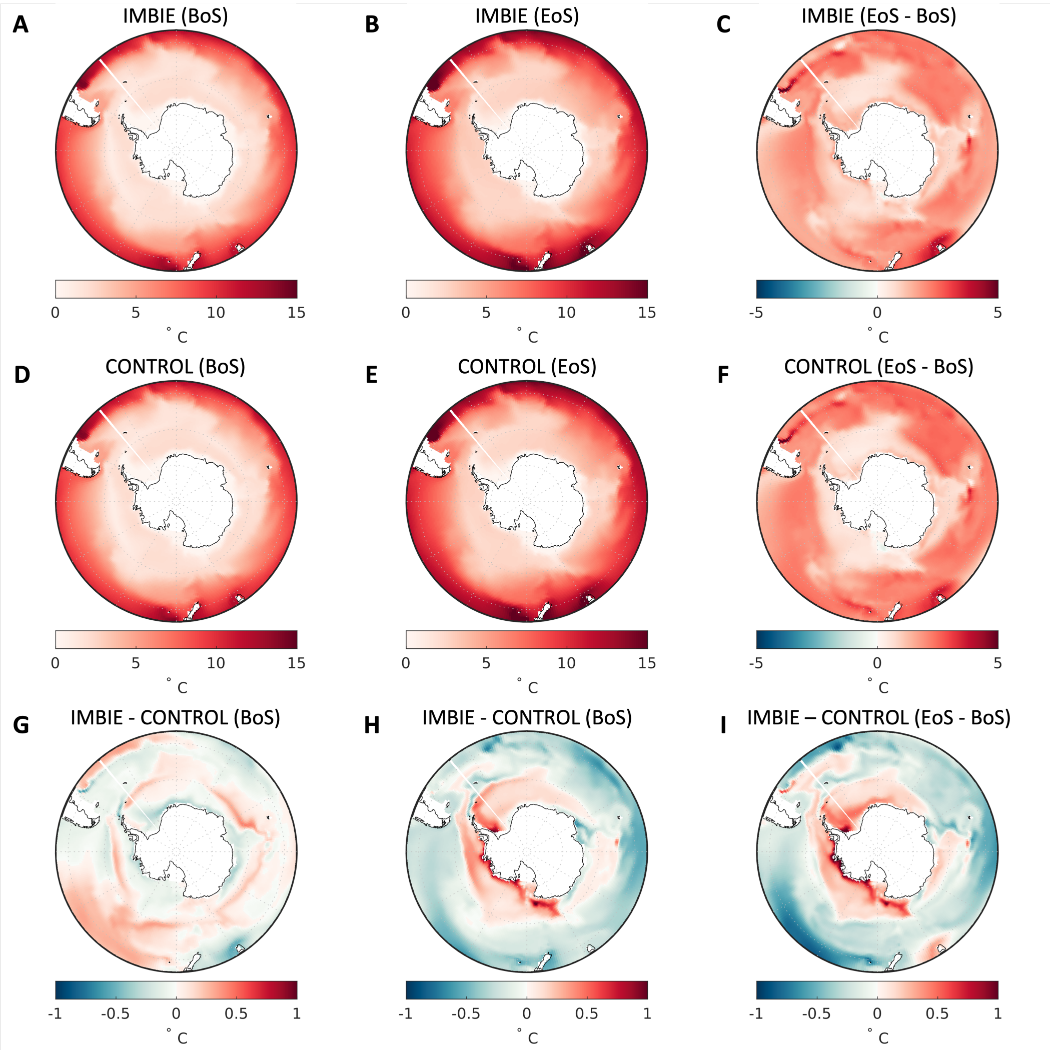

Figure S5. Snapshots of T_{200} for the IMBIE simulation (top row), CONTROL simulation (middle row), and the difference (IMBIE - CONTROL; bottom row). The columns depict the average T_{200} for the beginning of the simulation (BoS) from 1992-2007 (left), the end of the simulation (EoS) 2085-2100 (center), and the difference (right).

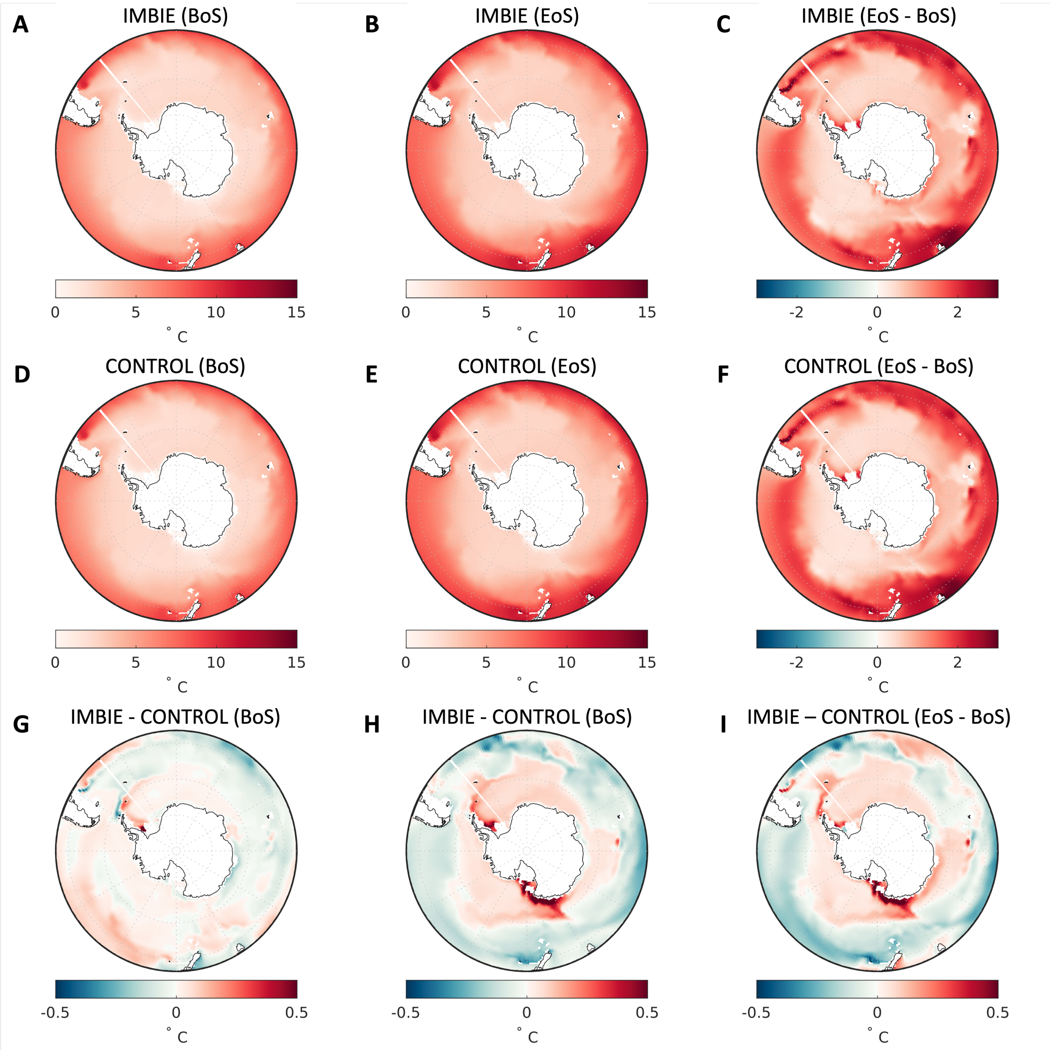

Figure S6. Snapshots of T_{500} for the IMBIE simulation (top row), CONTROL simulation (middle row), and the difference (IMBIE - CONTROL; bottom row). The columns depict the average T_{500} for the beginning of the simulation (BoS) from 1992-2007 (left), the end of the simulation (EoS) 2085-2100 (center), and the difference (right).

JOURNAL OF GEOPHYSICAL RESEARCH

Supporting Information for "Antarctic Ice Sheet freshwater discharge drives substantial Southern Ocean changes over the 21^{st} century"

Tessa Gorte[1,2], Nicole Lovenduski[1,2], Cara Nisssen [1,2], Jan Lenaerts[1], Leo van Kampenhout[3]

[1]University of Colorado Boulder

[2]Institute of Arctic and Alpine Research

[3]Utrecht University

Contents of this file

1. Freshwater forcing

2. Expanded results

0.1. Freshwater forcing

We define six drainage basins for the AIS: (1) the Weddell Sea, (2) the Indian Ocean, (3) the Pacific Ocean, (4) the Ross Sea, (5) the AB Seas, and (6) the Antarctic Peninsula, each of which produce different FW fluxes. The historical fluxes are taken from ? (?) which separates calving fluxes (solid ice) from basal melt fluxes (liquid water). Historically, calving and basal melt represent 48% and 52% of the total AIS FW flux, respectively, but this varies greatly from basin to basin. The FW forcing from the Antarctic Peninsula, for instance, is 13% calving and 87% basal melt compared to 74% calving and 26% basal melt for the Weddell Sea. Due to the sparse observations of AIS FW fluxes, we assume the calving to basal melt ratio persists into the future for every basin. The only drainage basin for which we adjust the FW discharge is the AB Seas basin which increases from 1992-2020 per a linear fit of the data published by ? (?). From 2021 through the end of the simulation period, we follow results from ? (?). By the end of the century, the AB Seas' flux increases from 716 Gt y^{-1} to 7039 Gt y^{-1} (still at a ratio of 32% calving to 68% basal melt).

0.2. Expanded results

For the first 15 years of the shared simulation period (1992-2007; beginning of simulation (BoS)) the upper ocean (top 200 m) stratification varies between 0-1 kg m^{-3} for both simulations. By the final 15 years (2085-2100, end of simulation (EoS)), the added FW engenders a $\sim$3 kg m^{-3} stronger stratification in the AB Seas region in the IMBIE simulation. Taking the difference in each simulation over time (Figure S2, panels C and F), we find that there is little difference in the CONTROL simulation while an increased stratification signal ($>$ 1 kg m^{-3}) manifests most strongly in the AB Seas and permeates into the Weddell and Ross Seas. With little change in the CONTROL simulation, the difference in the temporal evolution (Figure S2, panel I), then, shows a similar signal to that of the IMBIE simulation.

From the surface to (and below) 500 m, the SO warms ubiquitously. Close to the AIS, the surface SO is ∼0 °C at the BoS and increases to ∼2 °C by the EoS (Figure S3, panels A-F). Compared to the CONTROL, the IMBIE simulation produces a ∼ 0.3°C cooler surface ocean. Regions of anomalously cooler waters develop in the AB Seas region and off the coast of the Eastern AIS, near the historical sea ice edge (Figure S3, panel I). Like the surface, the temperature at 100 m depth (T_{100}) is also ∼0 °C at the BoS in both simulations and both warm over the 21^{st} century (Figure S4, panels A-F). Toward the EoS, the IMBIE simulation is anomalously warmer particularly close to the coast in the AB Seas region. This warming signal also manifests strongly (> 1 °C) in the Ross Sea and to a lesser extent (> 0.5 °C), in the Weddell Sea as well (Figure S4, panel I). The differences in temporal evolution of temperature at 200 m depth ($T_2 00$) between the two simulations becomes more spatially variable with anomalous cooling north of 60 °S and significant anomalous warming south of 60 °S (Figure S5, panels A-F). The strongest warming signals (> 1 °C) are close to the coast in the AB, Weddell, and Ross Seas as well as the Antarctic Peninsula. Offshore, there is further warming in excess of 0.25 °C all around the AIS including the Indian and Pacific Ocean drainage basins (Figure S5, panel I). 500 m below the surface is approximately the depth at which the entire zonally-averaged SO is warmer in the IMBIE than the CONTROL (Figure 4). At this depth, the historical temperatures (T_{500}) increase by 0.25-2 °C over the course of the century in both simulations. On the continental shelf and beyond, the IMBIE simulation traps significantly more heat than the CONTROL. This signal is particularly robust in the coastal western Ross Sea with differences exceeding 1 °C between the two simulations. As with T_{200}, offshore heat is trapped all around the AIS, extending out to nearly 45 °S in the southern Pacific and southern Atlantic Oceans.

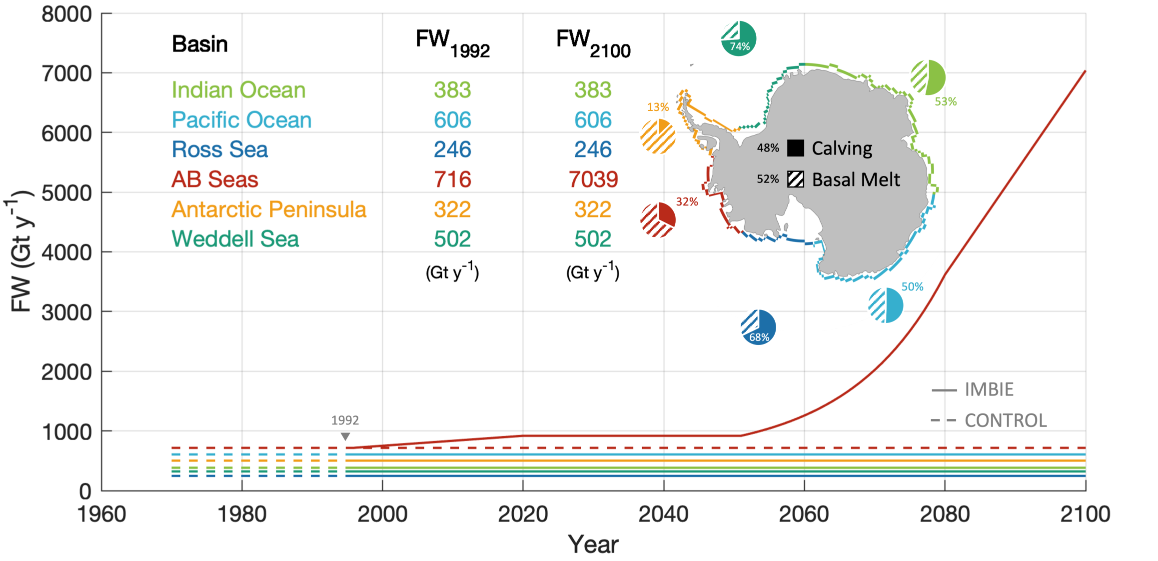

Figure S1. The AIS FW distribution shown spatially and as a time series. The 6 basins we define are the Weddell Sea (dark green), the Indian Ocean (light green), the Pacific Ocean (light blue), the Ross Sea (dark blue), the AB Seas (red), and the Antarctic Peninsula (orange). Each basin has its own ratio of calving to basal melt as depicted by the pie charts (percentages denote the percent of FW flux realized as calving). The time series show the total FW fluxing from each basin for the CONTROL (dashed) and the IMBIE (solid) simulations; the latter of which branches off in 1992. Also displayed are the values of total FW fluxing from each basin in 1992 and in 2100 in Gt y^{-1}.

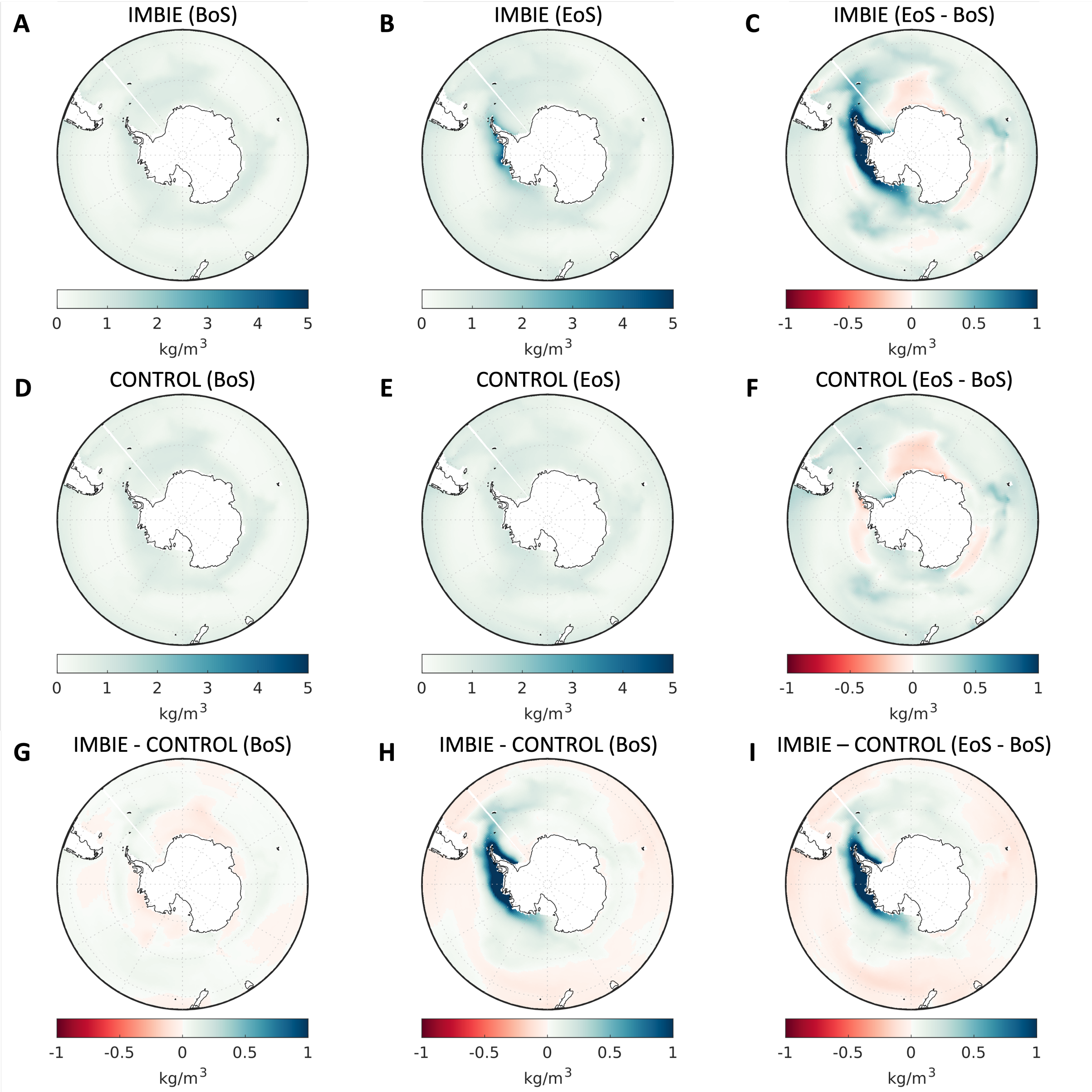

Figure S2. Snapshots of density stratification (200 m - surface) for the IMBIE simulation (top row), CONTROL simulation (middle row), and the difference (IMBIE - CONTROL; bottom row). The columns depict the average stratification for the periods of 1992-2007 (left), 2085-2100 (center), and the difference (right).

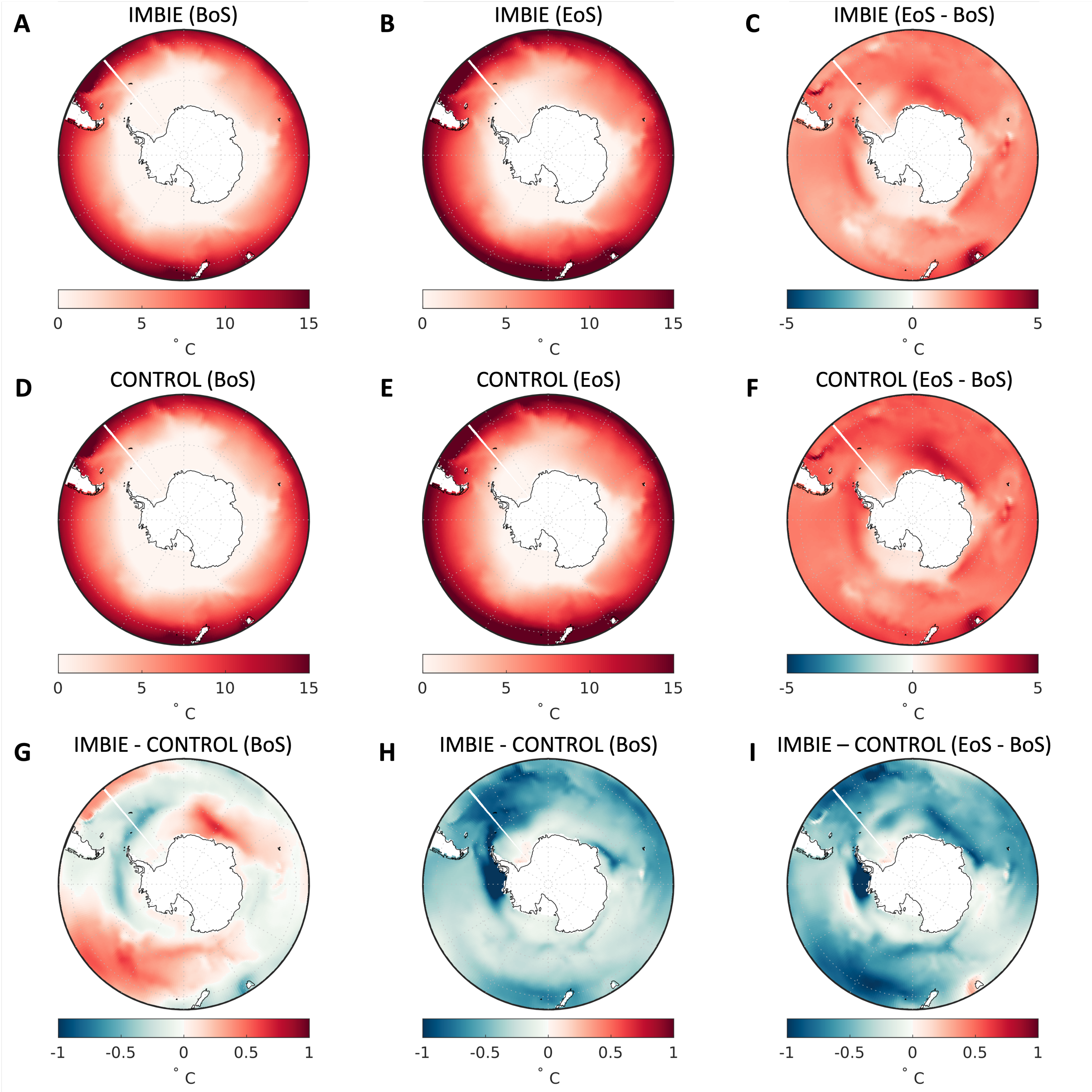

Figure S3. Snapshots of surface temperature for the IMBIE simulation (top row), CONTROL simulation (middle row), and the difference (IMBIE - CONTROL; bottom row). The columns depict the average surface temperature for the beginning of the simulation (BoS) from 1992-2007 (left), the end of the simulation (EoS) 2085-2100 (center), and the difference (right).

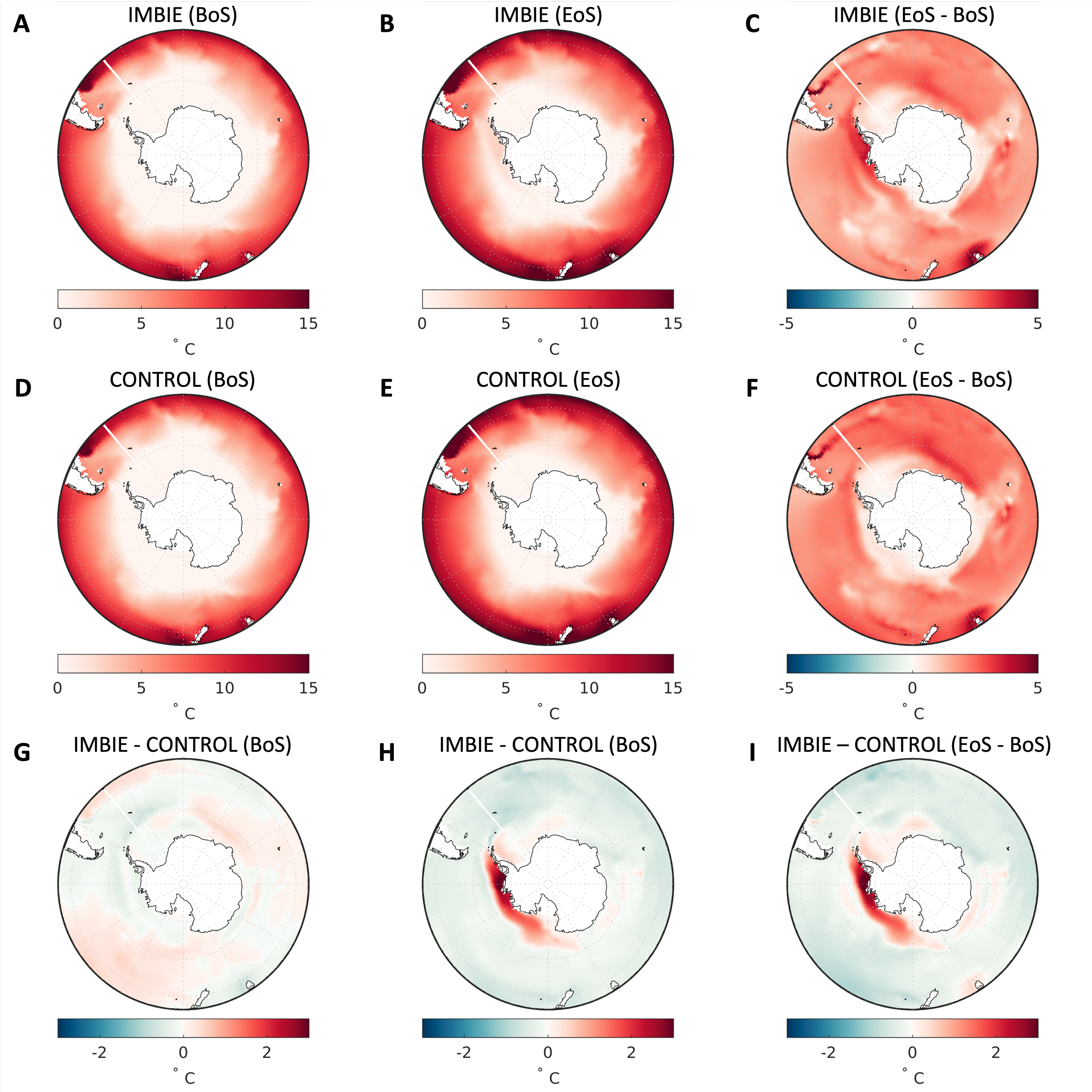

Figure S4. Snapshots of T_{100} for the IMBIE simulation (top row), CONTROL simulation (middle row), and the difference (IMBIE - CONTROL; bottom row). The columns depict the average T_{100} for the beginning of the simulation (BoS) from 1992-2007 (left), the end of the simulation (EoS) 2085-2100 (center), and the difference (right).

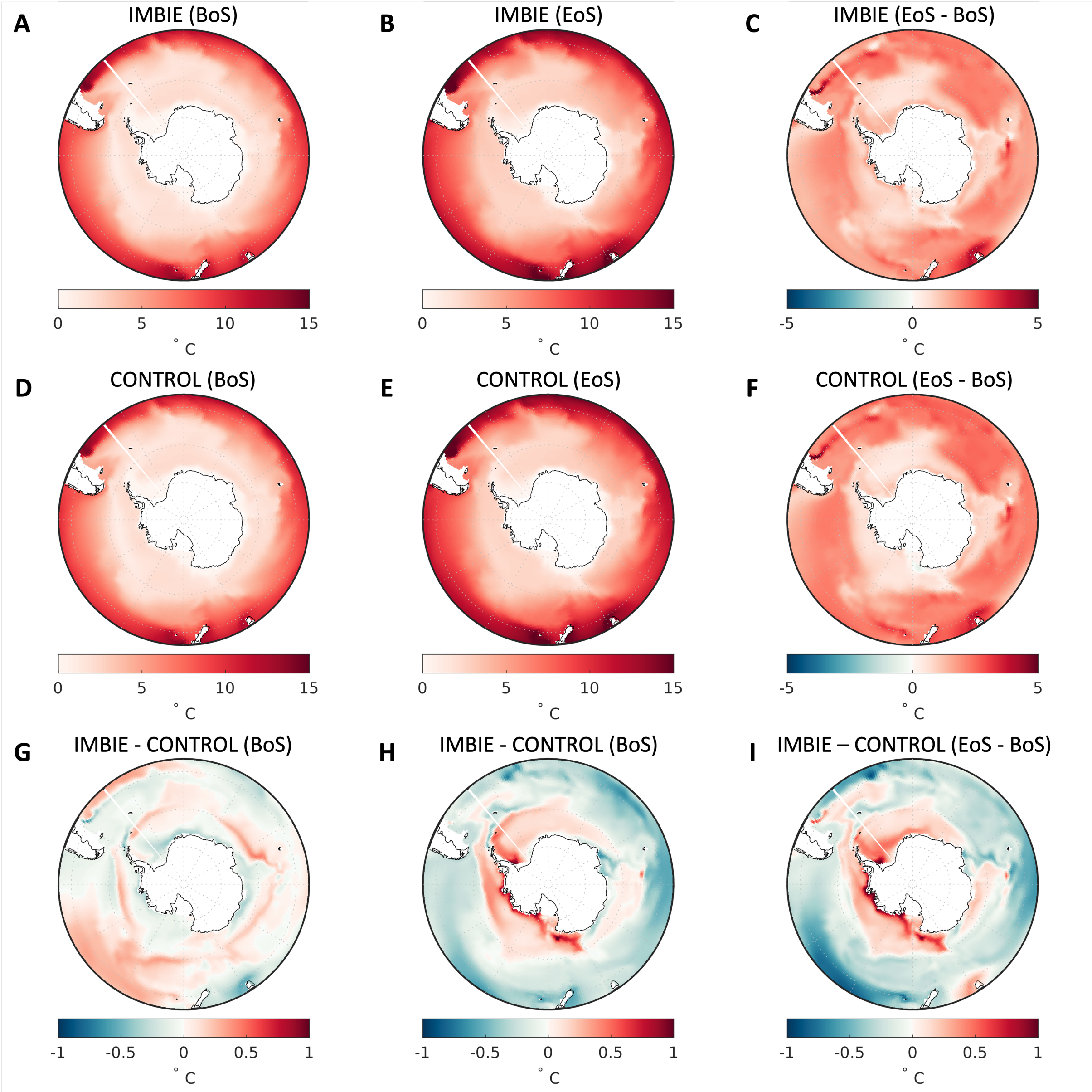

Figure S5. Snapshots of T_{200} for the IMBIE simulation (top row), CONTROL simulation (middle row), and the difference (IMBIE - CONTROL; bottom row). The columns depict the average T_{200} for the beginning of the simulation (BoS) from 1992-2007 (left), the end of the simulation (EoS) 2085-2100 (center), and the difference (right).

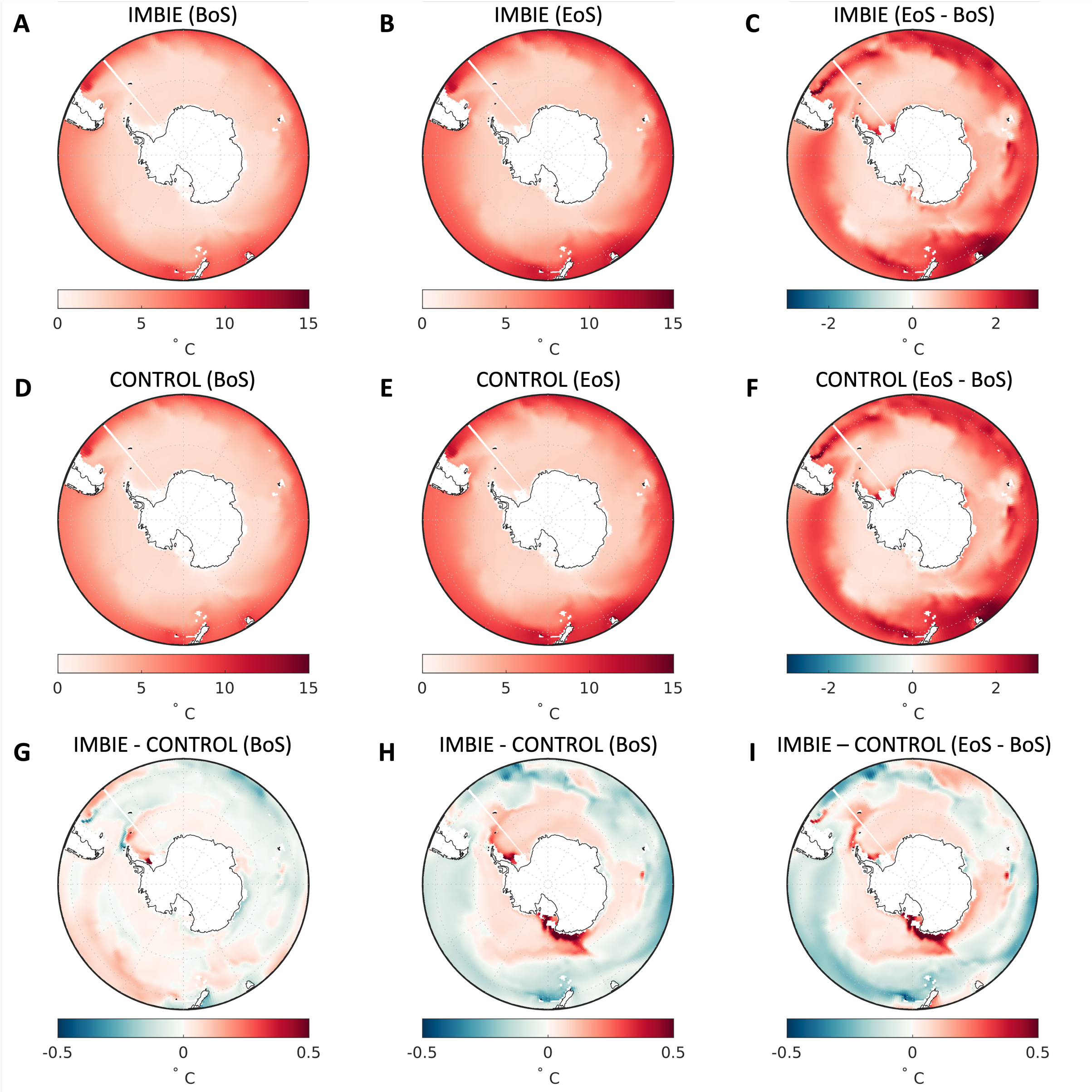

Figure S6. Snapshots of T_{500} for the IMBIE simulation (top row), CONTROL simulation (middle row), and the difference (IMBIE - CONTROL; bottom row). The columns depict the average T_{500} for the beginning of the simulation (BoS) from 1992-2007 (left), the end of the simulation (EoS) 2085-2100 (center), and the difference (right).